STRUCTURE, ELECTRONIC, AND PHOTOPHYSICAL PROPERTIES OF PLATINUM(II) BIPHENYL COMPLEXES CONTAINING 2,2'-BIPYRIDINE AND 1,10-PHENANTHROLINE DERIVATIVES

A Dissertation by

Wei Huang

B.S., Nanjing University, 1995

Submitted to the Department of Chemistry

and the faculty of the Graduate School of

Wichita State University

in partial fulfillment of

the requirements of the degree of

Doctor of Philosophy

December 2010

STRUCTURE, ELECTRONIC, AND PHOTOPHYSICAL PROPERTIES OF PLATINUM(II) BIPHENYL COMPLEXES CONTAINING 2,2'-BIPYRIDINE AND 1,10-PHENANTHROLINE DERIVATIVES

The following faculty members have examined the final copy of this dissertation for form and content, and recommend that it be accepted in partial fulfillment of the requirement for the degree of Doctor of Philosophy with a major in Chemistry

_____

Donald Paul Rillema, Committee Chair

_____

Bin Tang, Committee Member

_____

David Eichhorn, Committee Member

_____

Erach Talaty, Committee Member

Accepted for the College of Liberal Arts and Sciences

_____

William D. Bischoff, Dean

Accepted for the Graduate School

_____

J. David McDonald, Dean

DEDICATION

To my parents, my brother

and my dear friends

ACKNOWLEDGEMENTS

I would like to thank Dr. D. Paul Rillema for giving me the chance to work in his research group. All his advice, support, patience and guidance throughout the years helped me undertake the challenges in graduate research. I also thank my committee members – Dr. David Eichhorn, Dr. Erach Talaty, Dr. Melvin Zandler and Dr. Bin Tang for their support and helpful suggestions in preparation of this dissertation. I thank Dr. Khamis Siam for his work on DFT calculations, advice and encouragement. I also thank Dr. Arvin Cruz for his helpful suggestions. I thank Dr. David Eichhorn and Dr. Curtis Moore for the X-ray crystal structure determinations. I thank the Wichita State University Office of Research Administration, the Department of Energy, RSEC Grant and Parker Fellowships.

I am grateful for all my past and present colleagues in Dr. Rillema's research group who were very helpful during my studies. I also thank Qinhong Fu and Ningfeng Zhao for their help and friendship. I thank dearly my parents, Mengjian Huang and Yan Tian to whom this dissertation is dedicated as well as to my brother Ye Huang. I would also like to extend my gratitude to all my friends here in the US, especially Pastor San, Jin Zhong, Amy Qiao, Bobby Yang, Wenzhi Sun, Yong Zhou and Yinyin Wu.

Most of all, I thank God for all the things He brought into my life.

ABSTRACT

Platinum(II) biphenyl diimine complexes have been synthesized and characterized. Single crystal X-ray structures from seven complexes show two types of configurations about the platinum coordination sphere in the solid state: X and B (butterfly). The two configurations give different circular dichroism spectra (CD) based on their C_2 or C_s symmetry. The metal-to-ligand charge transfer (MLCT) bands which occur at ~440 nm are transitions from d orbitals on the platinum metal center to π^* orbitals of the diimine ligands. This agrees with the time dependant density functional theory (TDDFT) calculations where the lowest unoccupied molecular orbitals (LUMO) are located on diimine ligands.

Emission spectra of the complexes can be divided into three groups according to different emission excited states: group I, ligand centered transitions (LC); group II, ligand field transitions (LF) and group III, metal-to-ligand charge transfer (MLCT). Emission profiles from the groups are different from one another: LC transitions have vibronic structures; LF transitions have sharp peaks without vibronic structure and MLCT transitions have a broad peak without vibronic structure. Linear free energy correlations were found between emission maxims, reduction potentials and emission lifetimes with Hammett σ_p values. The diimine with electron donating substituents have the higher energy emission maxima and the longer emission life time. The diimine with electron withdrawing substituents has the lower energy emission maxima and the shorter emission life time.

TABLE OF CONTENTS

TABLE OF CONTENTS (continued)

LIST OF TABLES

LIST OF TABLES (continued)

LIST OF TABLES (continued)

LIST OF FIGURES

LIST OF FIGURES (continued)

LIST OF FIGURES (continued)

LIST OF FIGURES (continued)

LIST OF FIGURES (continued)

ABBREVIATIONS

3,4,7,8-Me_4phen	3,4,7,8-Tetramethyl-1,10-Phenanthroline
4,7-Me_2phen	4,7-Dimethyl-1,10-Phenanthroline
4,7-ph_2phen	4,7-Diphenyl-1,10-Phenanthroline
4-Mephen	4-Methyl-1,10-Phenanthroline
5,6-Me_2phen	5,6-Dimethyl-1,10-Phenanthroline
5-Clphen	5-Choloro-1,10-Phenanthroline
5-Mephen	5-Methyl-1,10-Phenanthroline
B3LYP	Becke-3-Parameter-Lee-Yang-Parr Exchange-Correlation Functional
bpy	2,2'-Bipyridine
CD	Circular Dichroism
DFT	Density Function Theory
HOMO	Highest Occupied Molecular Orbital
IC	Internal Conversion
IL	Intra-ligand
IR	Infrared Radiation
ISC	Intersystem Crossing
LC	Ligand Centered
LF	Ligand Field
LLCT	Ligand to Ligand Charge transfer
LUMO	Lowest Unoccupied Molecular Orbital
MLCT	Metal to Ligand Charge Transfer
NMR	Nuclear Magnetic Resonance
ORTEP	Orbital Representation Thermal Ellipsoid Plot

phen	1,10-Phenanthroline
SDD	Stuttart-Dresden
TDDFT	Time Dependent Density Function Theory
UV-vis	Ultra-Violet and Visible

CHAPTER 1

INTRODUCTION

1.1 Platinum(II) biphenyl diimine chemistry

Transition metal diimine complexes, i.e. $[Ru(bpy)_3]^{2+}$, $Re(bpy)(CO)_3Cl$ and $[Os(phen)_3]^{2+}$, have been studied for decades[1] for their excited state transient species and photoinduced electron transfer in applications such as solar energy conversion, photocatalysis, photonic molecular devices and photo luminescent probes of biological systems.[2-6] Research continues to focus on transition metal diimine complexes because they often possess long-lived excited states capable of bimolecular energy and electron transfer as well as efficient photoluminescence.

The main focus of this dissertation is the study of the excited states of platinum(II) biphenyl complexes containing a series substituted diimine ligands. Compared with the well-studied d^6 octahedral ruthenium(II) and rhenium(I) complexes, relatively little work has been done on d^8 square planar platinum(II) systems. The energy level of the metal-to-ligand charge transfer band (MLCT) increases in the series Ru(II) < Re(I) < Pt(II) providing a larger energy driving force for Pt(II) complexes.[1,7,8] Further, the biphenyl ligand has higher energy π and π^* orbitals driving up the excited state energy of the complex. Further, the biphenyl dianion assures a neutrally charged platinum(II) complex with diimine ligands which will be soluble in nonaqueous solvents. Ruthenium(II) and rhenium(I) complexes are charged limiting their solubility in similar solvent systems. Thus, platinum(II) biphenyl complexes overcome some of the difficulties found for other transition metal complexes and offer the opportunity of increasing the understanding of designing photocatalysts for solar energy conversion and other useful

purposes associated with light absorption. The preparation, absorption and emission spectra of platinum biphenyl diimine complexes will be discussed along with the results of Time Dependent Density Functional Theory (TDDFT) in the various chapters.

1.2 Emission and excited states

A photochemical process is initiated upon absorption of a photon by a molecule. This results in the excitation of an electron from the ground state to an excited state. The ground state is the stable electronic state having the lowest energy and is usually a singlet state. Excited states are unstable higher energy electronic states which relax to ground state by various pathways. The life time of the excited state is determined by the nature of the molecule, the type of excited states, as well as by the presence of quencher. Excited states often are either singlets or triplets.

Figure 1.1 shows the diagram of an emission process of a platinum diimine system. A platinum diimine molecule in its ground state S_0 undergoes an absorption process to a singlet excited state S_1. Then the excited molecule has three possible intersystem crossing (ISC) pathways to different triplet states: ligand centered (^{3}LC), ligand field (^{3}LF) and metal-to-ligand charge transfer (^{3}MLCT). Finally the molecule undergoes emission to the ground state.

Examples for the three types of decay to the ground state are: 1. cis-$Pt(NH_3)_2Cl_2$ has emission with a maximum near 17000 cm^{-1} (590 nm) attributed to decay from the ^{3}LF in a glassy matrix at 77K;[9] 2. $[Pt(bpy)(en)](ClO_4)_2$ has emission assigned from a ^{3}LC state having an origin at 458 nm with a vibronic pattern[10] of bipyridyl modes of 1400 cm^{-1} and 1000 cm^{-1}; 3. The emission from $[Ru(bpy)_3]Cl_2$ at 600 nm[16-18] is derived from a ^{3}MLCT state.

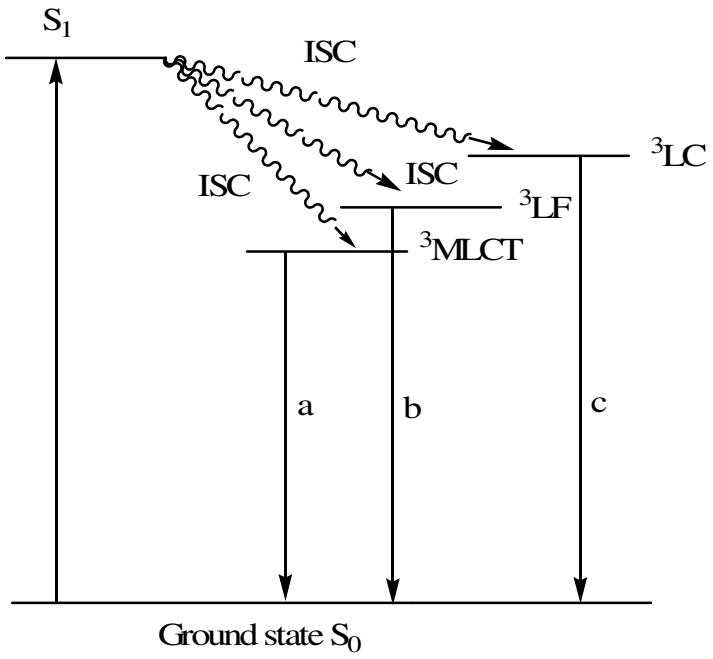

Figure 1.1 Emission process of a platinum diimine system

1.3 Hammett sigma values

1.3.1 Hammett equation

The Hammett equation in organic chemistry describes a linear free-energy relationship relating reaction rates and equilibrium constants for many reactions involving benzoic acid derivatives with *meta*- and *para*- substituents.[11, 12] The basis is summarized in equation (**1**),

$$\log \frac{K}{K_0} = \sigma\rho \qquad (\mathbf{1})$$

where K is the equilibrium constant for a reaction having a reactant with a substituent R (R ≠ H), K_0 is the equilibrium constant for the reaction when R = H, σ is the substituent constant for R and ρ depends only on the type of reaction, but not on the substituent used.

The equation also holds for reaction rates, k, of a series of reactions with substituted benzene derivatives by simple substitution of k for K as shown in equation (**2**). In this equation,

$$\log \frac{k}{k_0} = \sigma\rho. \qquad (2)$$

k_0 is the reaction rate constant containing the reactant with R = H, and k is the rate constant of the reaction where the substituent R attached to one of the reactants is varied.

A plot of $\log(K/K_0)$ for a given equilibrium versus $\log(k/k_0)$ for a given reaction rate with many differently substituted reactants gives a straight line.

1.3.2 Substituent constants

The starting point for the collection of the substituent constants is a chemical equilibrium for which both the substituent constant and the reaction constant are arbitrarily set to 1. This is taken to be the ionization of benzoic acid (R and R' both H) in water at 25°C.

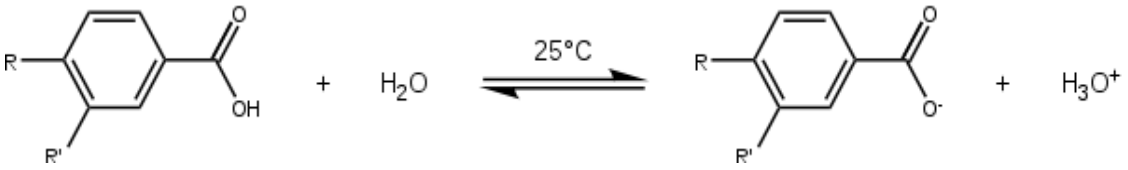

After obtaining a value for K_0, a series of equilibrium constants (K) are now determined based on the same process, but now with variation of the *para* substituent—for instance, p-hydroxybenzoic acid (R = OH, R' = H) or 4-aminobenzoic acid (R = NH_2, R' = H). These values, combined in the Hammett equation with K_0 and with ρ = 1, give the *para* substituent

constants σ_p. Similarly, σ_m values are obtained with *meta* substituents. Hammett sigma constants of some ordinary substituents are list in Table 1.1.

Table 1.1 Hammett sigma constants[13]

	σ_p	σ_m
H	0	0
CH_3	-0.17	-0.069
CH_2CH_3	-0.151	-0.07
C_6H_5	0.01	0.06
CN	0.66	0.56
CO_2CH_3	0.502	0.376
$CO_2CH_2CH_3$	0.45	0.37
Cl	0.227	0.373
NO_2	0.778	0.71

CHAPTER 2

STRUCTURE, ELECTRONIC, AND PHOTOPHYSICAL PROPERTIES OF PLATINUM(II) BIPHENYL COMPLEXES CONTAINING 2,2'-BIPYRIDINE AND 1,10-PHENANTHROLINE LIGANDS

2.1 Introduction

Platinum(II) biphenyl complexes have been synthesized through low-temperature procedures and studied since the 1980's.[14,15,19,20] These compounds show interesting photophysical properties. There are many similarities between platinum(II) biphenyl complexes and platinum diimine complexes, but the differences are also remarkable. Absorption and emission are sometimes hard to explain due to the multiple types of transitions in the system: IL, LLCT, MLCT and LF.[21]

In this paper, we report a modified synthetic procedure to prepare 2,2'-biphenyl-2,2'-bipyridyl platinum(II), [Pt(bph)(bpy)], and 2,2'-biphenyl-1,10-phenantroline platinum(II), [Pt(bph)(phen)], as well as [Pt(bph) $(CH_3CH_2)_2S]_2$. Crystal structures of the two complexes show different configurations. TDDFT calculations were used to help explain absorptions and emissions.

2.2 Experimental section

2.2.1 General procedures and chemicals

All syntheses were performed under a dry and oxygen-free nitrogen atmosphere using standard Schlenk-ware techniques. Anhydrous diethyl ether (99.7%) and anhydrous tetrahydrofuran, THF, (99.9%) were used as received from Aldrich. The other solvents, methylene chloride, hexanes, butyronitrile, etc., were used without further purification. Potassium tetrachloroplatinate(II) was purchased from Alfa Aesar. The ligand 2,2'-dipyridyl

was purchased from Acros and 1,10-phenanthroline monohydrate was purchased from GFS. Diethyl sulfide and n-butyl lithium were purchased from Aldrich.

2.2.2 Instrumentation and physical measurements

UV-Vis spectra were obtained using a Hewlett-Packard model 8452A diode array spectrophotometer interfaced with an OLIS software program. The IR spectra were acquired using a Nicolet Avatar 360 FT-IR spectrophotometer. Proton NMR spectra were obtained using a Varian Inova 400 FT-NMR spectrometer. Elemental (C, H, & N) analysis was performed by MHW Laboratories. An EG&G PAR model 263A potentiostat/galvanostat was used to obtain the cyclic voltammograms. The measurements were carried out in a typical H-cell using a platinum disk working electrode, a platinum wire counter electrode, and a Ag/AgCl reference electrode in acetonitrile. The supporting electrolyte used was 0.1M tetrabutylammonium hexafluorophosphate (TBAH). Ferrocene was added as the electrochemical reference.

Corrected emission spectra were collected using a Spex Tau3 Fluorometer. The excited state lifetimes were determined by exciting samples at 355 nm using an OPOTEK optical parametric oscillator pumped by a frequency tripled Continuum Surlite Nd:YAG laser. The emission curve-fittings were performed using the Origin 6.1 program by a non-the linear curve-fitting mode.

2.2.3 Calculations

Gaussian ’03 (Rev. B.03) software for UNIX was used for calculations. The molecules were optimized using Becke's three-parameter hybrid functional B3LYP[22] with the local term of Vosko, Wilk, and Nassiar. The basis set SDD[23] was chosen for all atoms and the geometry optimizations were all in the gas phase. TDDFT[24] calculations were employed to produce a

number of singlet excited states in the gas phase based on the optimized geometry. All vibrational analyses revealed no negative frequencies and were run in the gas phase only.

2.2.4 Preparation procedure

2.2.4.1 Preparation of 2,2'-dibromobiphenyl

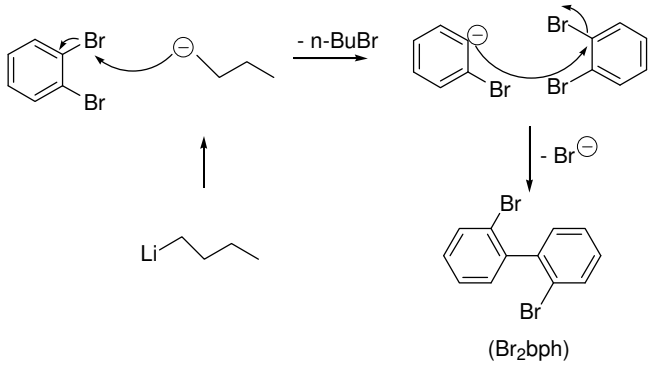

Figure 2.1 Preparation of 2,2'-dibromobiphenyl

2,2'-Dibromobiphenyl was prepared according to published procedures.[25] The mechanism of the reaction is shown in Figure 2.1. Dibromobenzene reacted with one equivalent of n-butyl lithium in dry ether to give the bromophenyl anion which then reacted with another equivalent of dibromobenzene to form the product.

2.2.4.2 Preparation of *cis*-$[PtCl_2(SEt_2)_2]$

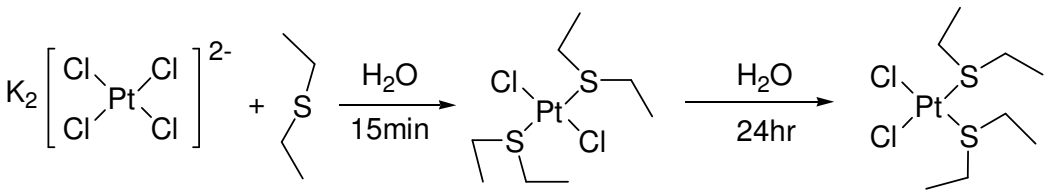

Figure 2.2 Preparation of *cis*-[$PtCl_2(SEt_2)_2$]

cis-[$PtCl_2(SEt_2)_2$] was prepared based on a published procedure.[26] $K_2[PtCl_4]$ reacted with diethyl sulfide in water. A yellow colored precipitate of *trans*-[$PtCl_2(SEt_2)_2$] was formed. After the mixture was stirred at room temperature for 24 hours, the initially formed *trans*-isomer was converted into the *cis*-isomer, which was soluble in water. The water was removed by evaporation to yield the *cis*-isomer product.

2.2.4.3 Preparation of $[Pt(bph)(SEt)_2]_2$

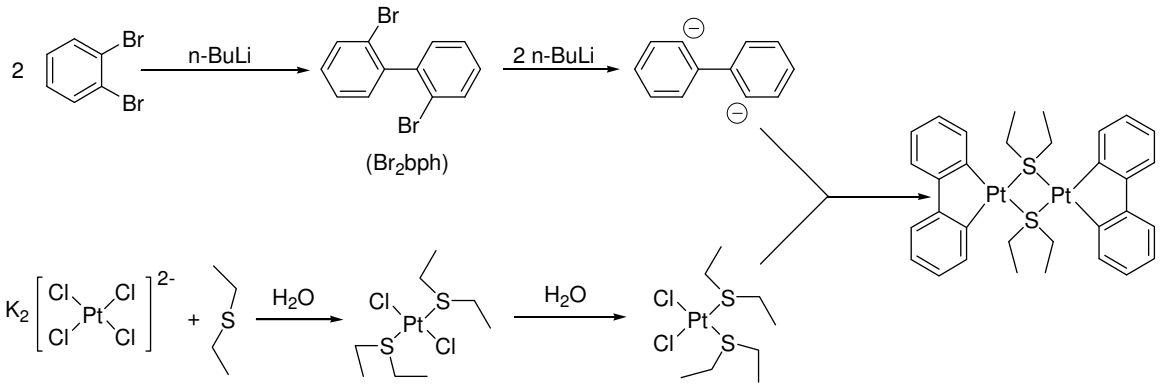

Figure 2.3 Preparation of $[Pt(bph)(SEt_2)]_2$

A modified preparation was used to obtain a higher yield compared to the published procedure[27]: The compound was prepared in two steps. First, the biphenyl dianion was prepared in Schlenk-ware consisting of a round-bottom flask connected by a T-tube to a dropping funnel. A serum cap was wired into place on the top of the T-tube containing 840 mg of 2,2'-

dibromobiphenyl (2.6 mmol) and a magnetic stir bar. Then the apparatus was evacuated three times and refilled with dry N_2 each time. Then 40 mL of dry ether was cannulated into the flask. The temperature of the contents of the flask was lowered to -70 °C with a dry ice/isopropanol bath. Then 2.1 mL of n-butyl lithium solution (2.5 M; 5.2 mmol) was added drop-wise using a gas tight syringe over a 2 h period. The solution containing the biphenyl dianion was then allowed to warm to 0°C for 2 h and then it was transferred to the dropping funnel which was connected to the T-tube.

For the second step, a second round-bottom flask containing 1.2 g $Pt((C_2H_5)_2S)_2Cl_2$ and a magnetic stir bar was fitted with a serum cap on top. The flask was evacuated three times and refilled with dry N_2 each time. Then about 40 mL of dry ether was cannulated into the flask. Then the dropping funnel from step one and the flask were rapidly connected, the system was flushed with N_2, partially evacuated (to not evaporate too much ether) two or three times and refilled with dry N_2 each time. The contents of the flask were cooled in an ethylene glycol-dry ice bath (-30°C to -40°C) and the contents of the dropping funnel were added over a 2 h period. Stirring was continued for an additional hour and then the contents of the flask were gradually warmed to ~0 °C and then to room temperature. The orange-brown colored suspension was filtered to remove the solids which yielded 0.32 g of yellow crystalline solid product upon extraction with methylene chloride. Another 0.25 g of product was obtained from the filtrate after hydrolysis of unreacted n-butyl lithium and/or the biphenyl dianion. Yield 49%.

2.2.4.4 Preparation of complexes

Pt(bph)(bpy)

A solution of 2,2'-dipyridyl (39 mg, 0.25 mmol) in methylene chloride (10 mL) was added drop-wise to a solution of $[Pt(bph)(C_2H_5)_2S]_2$ (100 mg, 0.114 mmole) in methylene

chloride (20 mL) under continuous stirring. The orange solution was stirred at room temperature for half hour and then rotary-evaporated to about 10 mL. The red crystals that formed were isolated and washed with ether. Yield 98 mg (90%). Anal. Calcd. for $C_{22}H_{16}N_2Pt$: C, 52.48; H, 3.20; N, 5.56. Found: C, 52.11; H, 3.09; N, 5.44. IR (KBr pellet): 3044, 1599, 1445, 1424, 1065, 738, 699 cm^{-1}. ^{1}H-NMR ($CDCl_3$): δ ppm 9.67 (d, 2H, J = 5.6 Hz), 8.18 (td, 2H, J = 5.6, 1.6 Hz), 8.13 (dd, 2H, J = 5.6, 1.6 Hz), 7.65 (td, 2H, J = 5.6, 1.6 Hz), 7.47 (dd, 2H, J = 6.8, 2.0 Hz), 7.39 (dd, 2H, J = 6.8, 2.0 Hz), 7.01 (td, 2H, J = 6.8, 2.0 Hz), 6.97 (td, 2H, J = 6.8, 2.0 Hz).

Pt(bph)(phen)

A solution of 1,10-phenanthroline (45 mg, 0.25 mmol) in methylene chloride (10 mL) was added drop-wise to a solution of $[Pt(bph)(C_2H_5)_2S]_2$ (100 mg, 0.114 mmole) in methylene chloride (20 mL) under continuous stirring. The orange solution was stirred at room temperature for ½ h and then rotary-evaporated to about 10 mL. The brown complex was isolated and washed with ether. Yield 110 mg (90%). Anal. Calcd. for $C_{24}H_{16}N_2Pt$: C, 54.65; H, 3.06; N, 5.31. Found: C, 54.45; H, 3.07; N, 5.27. IR (KBr pellet): 3041, 1653, 1581, 1426, 1419, 1021, 840, 743, 717 cm^{-1}. ^{1}H-NMR (CD_2Cl_2): δ ppm 9.93 (dd, 2H, J = 5.2, 1.2 Hz), 8.69 (dd, 2H, J = 8.0, 1.2 Hz), 8.02 (s, 2H), 8.00 (dd, 2H, J = 8.0, 5.2 Hz), 7.55 (dd, 2H, J = 6.8, 2.0 Hz), 7.34 (dd, 2H, J = 6.8, 2.0 Hz), 6.97 (m, 4H, J = 6.8, 2.0 Hz).

2.3 Results

2.3.1 X-Ray crystallographic data collection

The crystals were obtained by slow evaporation of saturated methylene chloride solutions. The unit cells were determined from the setting angles of 220 reflections for Pt(bph)(phen) and 276 reflections for Pt(bph)(bpy)) collected in 36 frames of data. Data were measured with a redundancy of 15.6 for Pt(bph)(phen) and 9.16 for Pt(bph)(bpy) using a CCD detector at a

distance of 40 mm for Pt(bph)(phen) and 50 mm for Pt(bph)(bpy) from the crystal with a combination of phi and omega scans. A scan width of 0.3 degrees for Pt(bph)(phen) and 0.5 degrees for Pt(bph)(bpy) and time of 10 seconds were employed along with graphite mono-chromated molybdenum Kα radiation (λ= 0.71073 Å) that was collimated to a 0.3 mm diameter for Pt(bph)(phen) and a 0.6 mm diameter for Pt(bph)(bpy). Data collection, reduction, structure solution, and refinement were performed using the Bruker Apex2 suite (v2.0-2).[28] All available reflections to 2θmax = 52° were harvested (47701 for Pt(bph)(phen) and 127510 for Pt(bph)(bpy), 3311 unique for Pt(bph)(phen) and 7131 unique for Pt(bph)(bpy)) and corrected for Lorentz and polarization factors with Bruker SAINT (v6.45).[28] Reflections were then corrected for absorption (numerical correction, μ = 7.414 mm^{-1}), interframe scaling, and other systematic errors with SADABS 2004/1 (combined transmission and other correction factors min/max = 0.2692/0.4457 for Pt(bph)(phen) and 0.3009/0.7994 for Pt(bph)(bpy)). The structures were solved (direct methods) and refined (full-matrix least-squares against F^2) with the Bruker SHELXTL package (v6.14-1).[28] All non-hydrogen atoms were refined using anisotropic thermal parameters. All hydrogen atoms were included at idealized positions; hydrogen atoms were not refined. Pertinent crystal, data collection, and refinement parameters are given in Table 2.1. The compound Pt(bph)(phen) sits on a general position in the monoclinic space group $P2_1/c$ and Pt(bph)(bpy) in the tetragonal space group $I4_1/a$. Selected bond distances and angles are provided in Table 2.2. ORTEP diagrams are shown in Figure 2.4.

Table 2.1 Crystal data and structure refinement for Pt(bph)(phen) and Pt(bph)(bpy)

complex	Pt(bph)(phen)	Pt(bph)(bpy)
Empirical formula	$C_{24}H_{16}N_2Pt_1$	$C_{22}H_{16}N_2Pt_1$
Formula weight	527.48	503.45
Temperature	150 K	150 K
Wavelength	0.71073 Å	0.71073 Å
Crystal system	Monoclinic	Tetragonal
Space group	$P2_1/c$	$I4_1/a$
Unit cell dimensions	a = 10.1828(6) Å	a = 38.6769(7) Å
	b = 13.9182(8) Å	b = 38.6769(7) Å
	c = 12.8693(7) Å	c = 9.7217(4) Å
	α = 90°	α = 90°
	β = 112.509(3)°	β = 90°
	γ = 90°	γ = 90°
Volume	1684.97(17) $Å^3$	14542.7(7) $Å^3$
Z	4	32
Calculated density	2.079 g/cm^3	1.838 g/cm^3
Absorption coefficient	8.338 mm^{-1}	7.724 mm^{-1}
F(000)	1008	7664
Crystal size	0.24 x 0.18 x 0.16 mm	0.19 x 0.06 x 0.04 mm
Crystal habit	Block	Prism
Crystal color	Lustrous Dark Purple	Lustrous Dark Red
θ range for data collection	2.25° to 26.00°	3.16 ° to 26.00°
Limiting indices	$-12 \leq h \leq 12$	$-47 \leq h \leq 47$
Reflections collected / unique	47701 / 3311 [R(int) = 0.0494]	127510 / 7131 [R(int) = 0.1114]
Completeness to θ = 26.00	100 %	99.8 %
Refinement method	Full-matrix least-squares on F^2	Full-matrix least-squares on F^2
Data / restraints / parameters	3311 / 0 / 244	7131 / 0 / 451
Refinement threshold	$I>2\sigma(I)$	$I>2\sigma(I)$
Data > threshold	2986	5039
Goodness-of-fit on F^2	1.059	1.091
Final R indices [$I>2\sigma(I)$]	R1 = 0.0156, wR2 = 0.0335	R1 = 0.0539, wR2 = 0.1229
R indices (all data)	R1 = 0.0193, wR2 = 0.0347	R1 = 0.0891, wR2 = 0.1375
Largest diff. peak and hole	0.727 and -0.603 $e^- Å^{-3}$	2.325 and -1.086 $e^- Å^{-3}$

2.3.2 X-Ray Crystal structure determination and DFT optimization

Figure 2.4 shows the structures of [Pt(bph)(bpy)] and [Pt(bph)(phen)] determined by X-ray crystallography. Selected bond distances and angles are given in Table 2.2 as well as the values from calculations. Bond lengths of platinum to carbon and to nitrogen atoms were between 1.99~2.01 Å and 2.10~2.12 Å, respectively, which were normal compared to those of similar complexes.[14, 29-33] The coordination sphere of platinum was not perfectly square planar in [Pt(bph)(bpy)]. A 26° C-C-N-N torsion angle gave it an X shape configuration as shown in Figure 2.4. On the other hand, the coordination sphere of [Pt(bph)(phen)] was square planar, but the bph and phen ligands wings were slightly bent in opposite directions, which gave a butterfly-like configuration. Both complexes were stacked in pairs in the solid state. The distances between platinum-platinum centers were 3.505 Å in [Pt(bph)(bpy)] and 3.387 Å in [Pt(bph)(phen)]. Calculated structures were optimized from DFT calculation with the B3LYP/SDD basis set. The configurations were set to X or butterfly according to crystal structures. The calculated parameters agree with the values from the crystal very well.

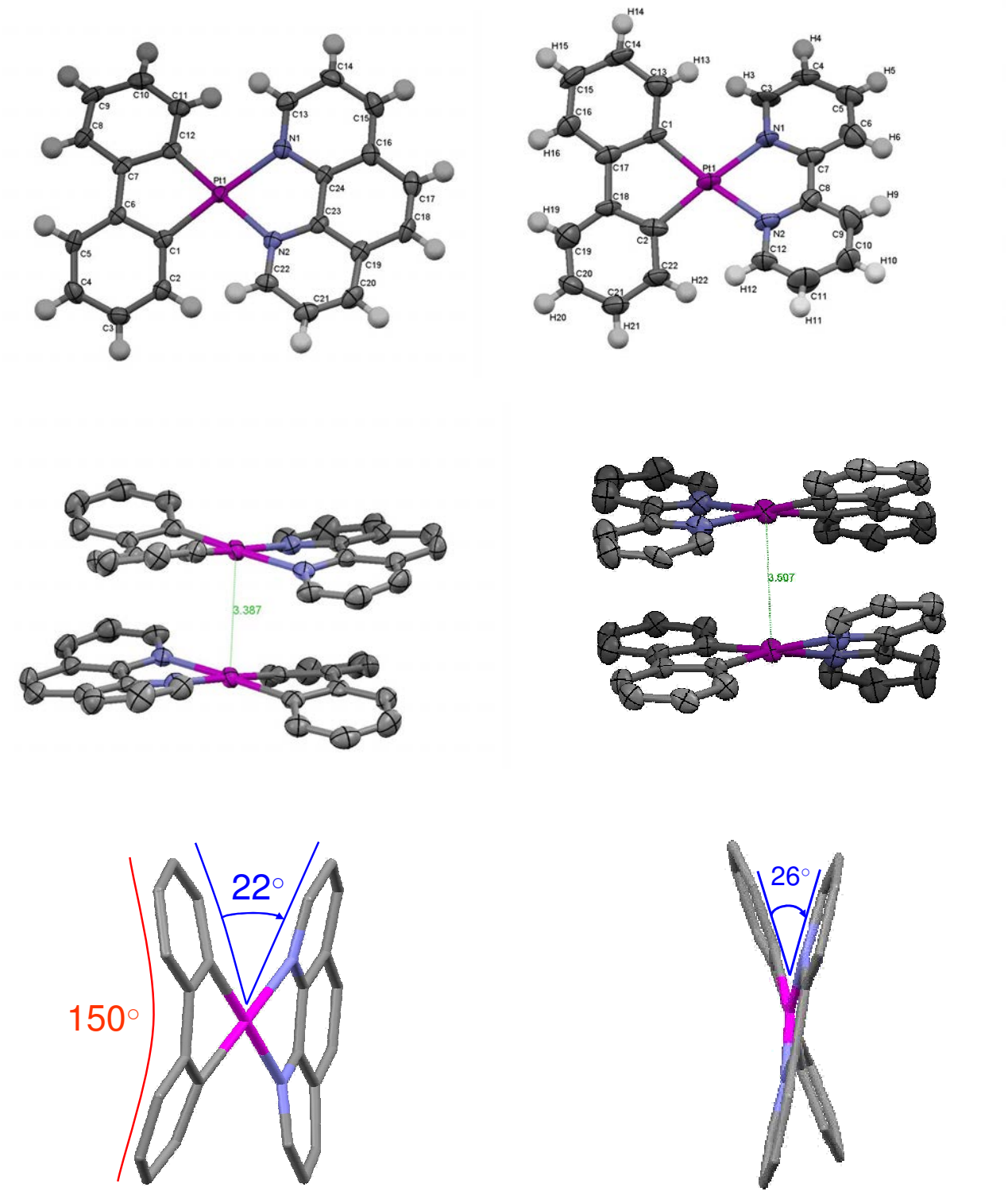

Figure 2.4 ORTEP diagrams and structures of [Pt(bph)(bpy)] and [Pt(bph)(phen)]

Table 2.2 Selected bond lengths (Å) and angles (deg) for Pt(bph)(phen) and Pt(bph)(bpy)

Pt(bph)bpy	Crystal	Calc.	Pt(bph)phen	Crystal	Calc.
Bond length (Å)			Bond length (Å)		
Pt-N1	2.116	2.154	Pt-N1	2.122	2.17
Pt-N2	2.095	2.154	Pt-N2	2.121	2.17
Pt-C1	2.015	2.032	Pt-C1	1.991	2.033
Pt-C12	1.99	2.032	Pt-C12	2.005	2.033
Bond angle (deg)			Bond angle (deg)		
C1-Pt-C12	80.74	80.68	C1-Pt-C12	80.46	80.1
N1-Pt-N2	78.23	76.4	N1-Pt-N2	77.61	76.7
C1-Pt-N1	102.75	103.6	C1-Pt-N1	101.46	101.5
C12-Pt-N2	101.89	103.6	C12-Pt-N2	100.36	101.5
Dihedral (deg)			Dihedral (deg)		
Pt-C-C-bph *	176.35	179	Pt-C-C-bph *	162.74	160.4
Pt-N-N-bpy *	179.73	176.3	Pt-N-N-phen *	163.15	168.7
C-C-N-N	20.2	30	C-C-N-N	0.33	0.004
Pt-Pt distance (Å)	3.505	---	Pt-Pt distance (Å)	3.387	---

2.3.3 Electronic absorption spectra

Complexes [Pt(bph)(bpy)] and [Pt(bph)(phen)] gave similar UV-Vis spectra. Figure 2.5 shows the absorption spectra in acetonitrile. The absorption coefficients of the transitions were

determined from Beer's Law studies using five dilution points and are listed in Table 2.3. There are three bands located as follows: 400-500 nm, 290-350 nm and a strong absorption band < 290 nm. The possible assignments of the experimental bands were based on computational assignments of the singlet excited states and related reports of similar types of complexes. The band at 440 nm is assigned as MLCT. The band at 260 nm is labeled LC. The bands located in the 290-350 nm region are more difficult to assign and it will be discussed later.

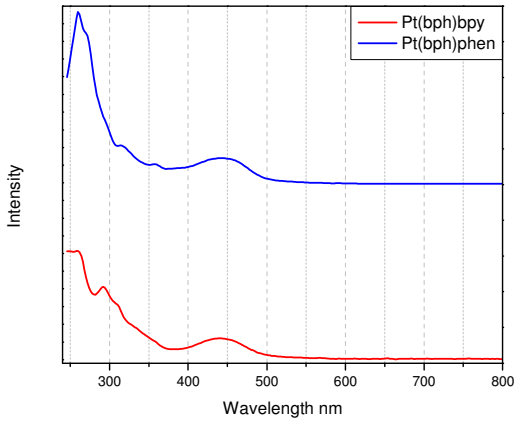

Figure 2.5 UV/Vis spectra of Pt(bph)(phen) and Pt(bph)(bpy)

Table 2.3 Absorption and emission spectral data

	λ_{abs} nm		λ_{em} nm	Φ_{em}	$\tau(\mu s)$	$E_{1/2red}(v)$
	IL	MLCT	(77K)	(10^{-4})		
Pt(bph)bpy	260 (1.5 x 10^4) 292 (9.9 x 10^3) 312 (7.2 x 10^3)	440 (2.9 x 10^3)	488	38	3.34	-1.402
Pt(bph)phen	262 (5.5 x 10^4) 314 (1.2 x 10^4) 358 (6.5 x 10^3)	442 (8.4 x 10^3)	586	26	1.1^{14}	-1.374

2.3.4 Emission properties and excited state lifetimes

Figure 2.6 and 2.7 show emission spectra in butyronitrile at 77 K. [Pt(bph)(bpy)] gave vibronic fine structure with λ_{max} at 488 nm; on the other hand, the emission maximum for [Pt(bph)(phen)] was located at 600 nm with no vibronic structure.

After the wavelength values were converted to energy, the emission spectral data were fitted to equation **3**, where the summation was carried out over the two sets of six vibrational levels.[15] The parameters were as follows: I_0 was base line, A was the peak area, n_1, n_2 = 0 to 5,

$$I(E) = I_0 + A[\Sigma_{n1}\,\Sigma_{n2}\,[(E_0 - n_1\hbar\omega_1 - n_2\hbar\omega_2) / E_0]^4\,(S_1^{n1}/ n_1!)\,(S_2^{n2}/ n_2!)$$

$$\exp\{-4 \log 2\,[(E - E_0 + n_1\hbar\omega_1 + n_2\hbar\omega_2) / \upsilon_{1/2}]^2\}] \qquad (\mathbf{3})$$

E_0 was the zero-zero energy, $\hbar\omega_1$ and $\hbar\omega_2$ represented the energies of the high and low vibrational frequency acceptor modes, S_1 and S_2 were the measures of the distortion in the high and low frequency acceptor modes and $\upsilon_{1/2}$ was the full-width at half-maximum of the zero-zero

vibronic component in the emission spectra. The maximum intensity was adjusted to 1 for the curve fitting analysis.

The spatial distribution of the singly occupied orbitals in the excited state can be determined from the vibrational frequency acceptor modes. Example: for the LC state the high frequency acceptor mode would be the ligand ring breathing mode. The coefficients S_1 and S_2 are indicative of the relative contributions of the high and the low vibrational modes to the fine vibronic structure of the emission.

The results of the emission spectral curve fitting at 77 K (Figures 2.6 and 2.7) are listed in Table 2.4. The values of the high frequency modes at about 1500 cm^{-1} correspond to ring breathing modes for the complexes and were consistent with the location of the low lying excited state on the bpy ligand. The low frequency modes were attributed to metal-ligand vibrations.

Table 2.4 Emission spectral curve fitting parameters of Pt(bph)(bpy) and Pt(bph)(phen) in butyronitrile at 77 K

	Pt(bph)(bpy)	Pt(bph)(phen)
E_0 (cm^{-1})	20640 ±160	17788 ±47
$\hbar\omega_1$ (cm^{-1})	1350 ±14	1159 ±22
$\hbar\omega_2$ (cm^{-1})	471 ±19	286 ±14
S_1	1.2 ±0.03	0.56 ±0.025
S_2	0.66 ±0.05	2.32 ±0.2
$\upsilon_{1/2}$ (cm^{-1})	932 ±170	862 ±55
I_0	0	0
A	0.668 ±0.26	0.256 ±0.02

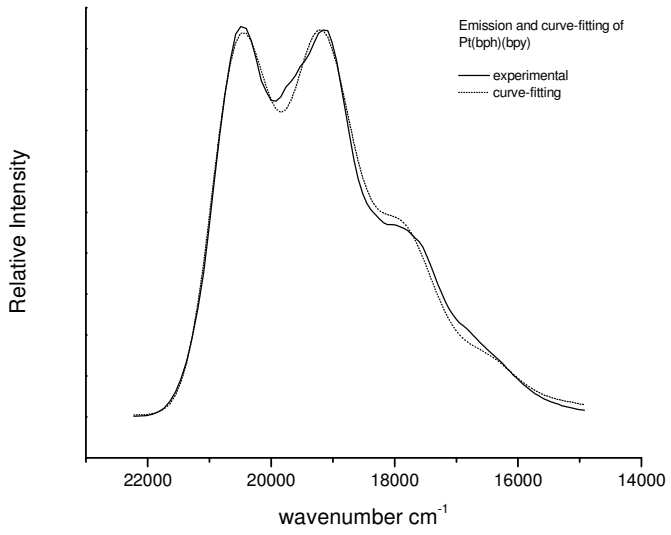

Figure 2.6 Emission spectra of [Pt(bph)(bpy)] at 77K (solid) and curve fitting (dot)

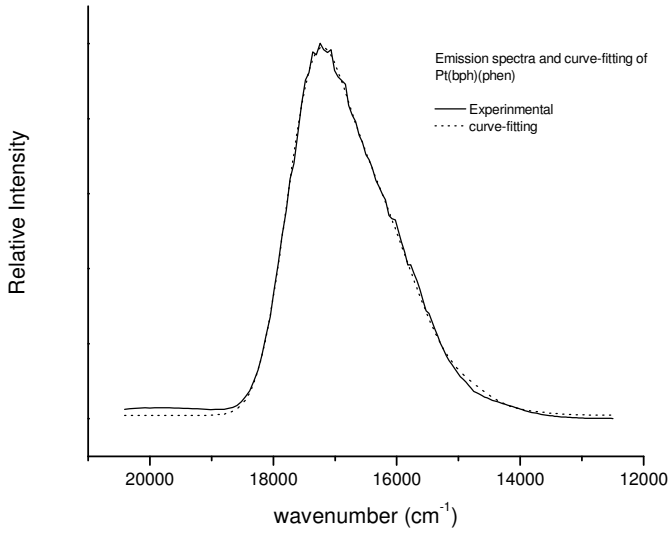

Figure 2.7 Emission spectra of [Pt(bph)(phen)] at 77 K (solid) and curve fitting (dot)

2.4 Discussion

2.4.1 Synthesis

Modification of the procedure for the synthesis of $[Pt(bph)(CH_3CH_2)_2S]_2$ gave a remarkable improvement in product yield[1] from17% to 49%. The temperature control and slow warming process seems to be critical in this reaction. On preparation of Pt(bph)(phen) and Pt(bph)(bpy), instead of adding $[Pt(bph)(CH_3CH_2)_2S]_2$ into melted bpy or phen, the reaction was carried out in methylene chloride.

2.4.2 Structures

It is very interesting that two similar complexes have different coordination sphere configurations in the solid state. In Figure 2.4 Pt(bph)(phen) has a butterfly (bowlike), B, configuration as in $Pt(bpy)_2(TCNQ)_3$[32] and $Pt(bpy)_2(TCNQ)_2$.[31] Pt(bph)(bpy) has the X configuration as in $Pt(phen)Cl_2$[33] and $Pd(phen)_2(ClO_4)_2$,[37] The tetrahedral distortion angle of Pt(bph)(bpy) in the X configuration is 26° compared with 24° in $Pt(bpy)_2(NO_3)_2 \cdot H_2O$.[36] In Figure 2.4 X has C_2 symmetry which is optically active and B has a C_s symmetry which is optically inactive. However, as noted in Figure 2.8, both complexes are optically active with opposite optical rotations. Calculations shown for the X and B forms of Pt(bpy)(phen) in Figure 2.9 are consistent with its found rotation as the B isomer.

In the optimization process we tried different bases sets, MP2/SDD, MP2/LanL2DZ and DFT/SDD, to check which configuration gave the lower energy. According to the results, the X form always had lower energy than the B form in Pt(bph)(phen) and Pt(bph)(bpy). The energy for the Pt(bph)(phen) X form were 1.79 x 10^{-3} eV (MP2/SDD), 2.42 x 10^{-3} eV (MP2/LanL2DZ) and 2.88 x 10^{-3} eV (DFT/SDD) and for the B form were 2.88 x 10^{-3} eV (MP2/SDD), 2.84 x 10^{-3} eV (MP2/LanL2DZ) and 3.59 x 10^{-3} eV (DFT/SDD).

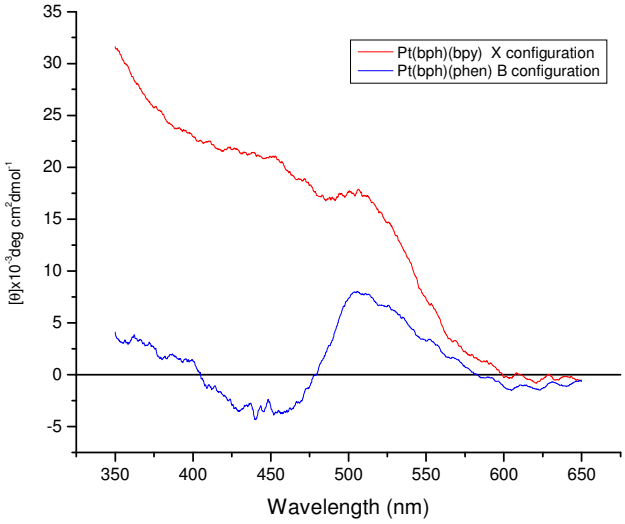

Figure 2.8 Circular dichroism spectra of Pt(bph)(bpy) and Pt(bph)(phen)

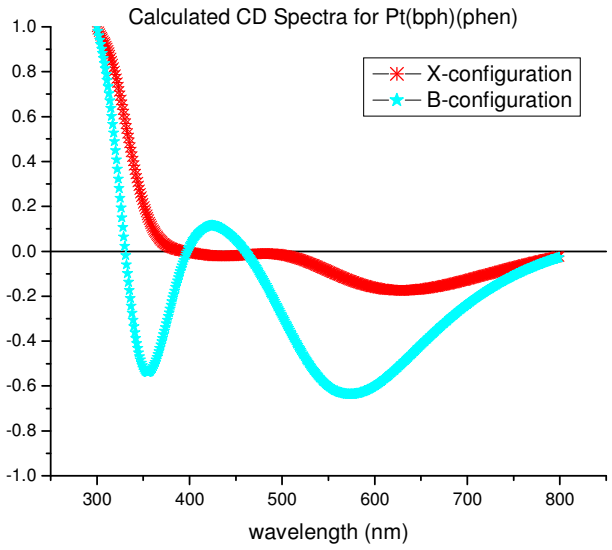

Figure 2.9 Calculated circular dichroism spectra of Pt(bph)(phen) with X and B configuration

In the solid state, both complexes form dimeric units. The intermolecular distance from platinum to platinum is 3.505 Å for Pt(bph)(bpy) and 3.387 Å for Pt(bph)(phen) which can be compared to the famous yellow-red form of Pt(bpy)Cl2 where the Pt-Pt distance is 3.40 Å for red

form and 4.435 Å for the yellow form.18 It is very likely there is a weak metal-to-metal interaction in the solid state.

2.4.3. Population analysis

2.4.3.1 [Pt(bph)(bpy)]

Figure 2.10 shows pictures of orbitals from HOMO-3 to LUMO+3. The orbital distribution and calculated singlet energy state transitions are listed in Table 2.5 and Table 2.6. HOMO and HOMO-5 are π orbitals from bph ligand. From HOMO-1 to HOMO-4, orbitals are mainly distributed on the platinum metal center and bph ligand. LUMO to LUMO+3 are π^* orbitals of the bpy ligand. LUMO+4 is a π^* orbital from bph and in LUMO+5 the electron density is 100% on platinum metal center.

Three dominant transitions are located at 17880 cm^{-1}, 36493 cm^{-1}, and 39818 cm^{-1}. The one located at 17880 cm^{-1} is a MLCT band associated with a platinum metal center to bpy ligand transition, H-1→LUMO (f = 0.0994). The 36493 cm^{-1} absorption is an IL ($\pi\rightarrow\pi^*$) transition located on bpy, H-10→LUMO (f = 0.2409). The 39818 cm^{-1} transition is associated with an IL ($\pi\rightarrow\pi^*$) transition located on bph, H-2→L+4 (f = 0.4028). There are some other interesting transitions with weak oscillator strengths, eg. a LLCT ($\pi\rightarrow\pi^*$) assigned as bph→bpy at 20035 cm^{-1}, HOMO→L+2 (f = 0.0444), and a MLCT band associated with Pt→bpy at 24155 cm^{-1}, H-1→L+1 (f = 0.0477).

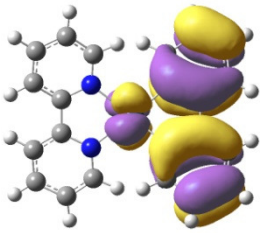

HOMO

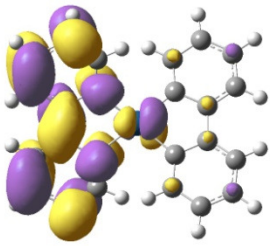

LUMO

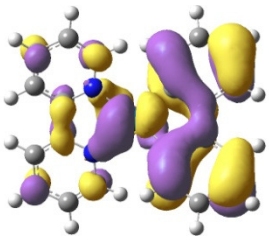

H-1

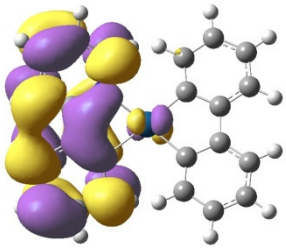

L+1

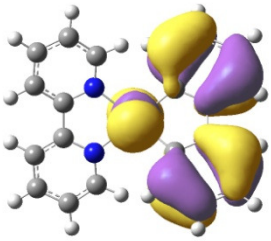

H-2

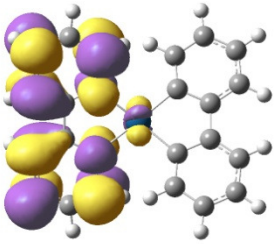

L+2

Figure 2.10 Frontior orbitals of Pt(bph)(bpy)

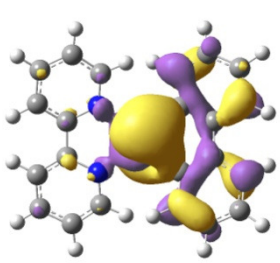

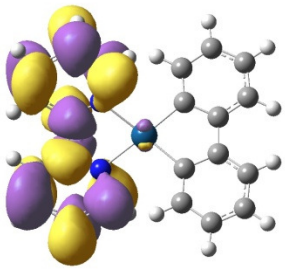

H-3 L+3

Figure 2.10 Molecular orbitals of Pt(bph)(phen) (continued)

Table 2.5 Orbital distributions of Pt(bph)(bpy) from calculations

	Energy level (eV)	Pt%	Bph%	Bpy%
LUMO+5	0.02	100	1	-1
LUMO+4	-0.27	9	89	2
LUMO+3	-0.42	1	0	99
LUMO+2	-1.7	1	1	98
LUMO+1	-1.84	2	1	97
LUMO	-2.7	5	3	92
HOMO	-4.71	19	80	1
HOMO-1	-5.41	38	51	12
HOMO-2	-5.58	28	71	1
HOMO-3	-5.59	71	26	2
HOMO-4	-6.48	67	26	7
HOMO-5	-6.61	16	78	6

Table 2.6 Calculated singlet energy state transitions for Pt(bph)(bpy)

ν(cm^{-1})	λ(nm)	f	Major orbital contributions	Nature of transition
17884	559.13	0.0994	H-1→LUMO (80%)	MLCT Pt→bpy
20035	499.11	0.0444	HOMO→L+2 (87%)	LLCT bph→bpy
24155	413.99	0.0477	H-1→L+1 (86%)	MLCT Pt→bpy
30344	329.55	0.0492	H→L+4 (81%)	ILπ→π* bph
33298	300.31	0.0459	H-9→LUMO (44%), H-4→L+2 (33%)	MLCT, LLCT Pt,bph→bpy
36493	274.02	0.2409	H-10→LUMO (54%)	ILπ→π* bpy
39818	251.14	0.4029	H-2→L+4 (41%)	ILπ→π* bph
40325	247.98	0.0876	H-9→L+1 (28%), H-3→L+5 (29%)	LF Pt d→p?

2.4.3.2 [Pt(bph)(phen)]

Figure 2.11 shows pictures of orbitals from HOMO-3 to LUMO+3. The orbital distribution and calculated singlet energy state transitions are listed in Table 2.7 and Table 2.8. The frontier orbitals are quite similar to those of Pt(bph)(bpy). The HOMO and HOMO-3 are derived from bph π orbitals. The HOMO-1, HOMO-2, HOMO-4 and HOMO-5 orbitals are mainly distributed on the platinum metal center and bph ligand. The LUMO to LUMO+3 are π* orbitals derived from the phen ligand. The principle component of LUMO+4 are the π* orbitals from bph and the principle component for LUMO+5 are the d orbitals from platinum.

The predominant transitions are: 18606 cm^{-1} assigned as H-1→LUMO (f = 0.1373), 37810 cm^{-1} assigned as H-11→L+1 (f = 0.1136), and 39235 cm^{-1} labeled as H-11→LUMO (f = 0.1618). The low energy transition is a MLCT band resulting from an electronic tansition from the platinum metal center to the phen ligand. The latter two are IL (π→π*) transitions associted with phen and bph, respectively.

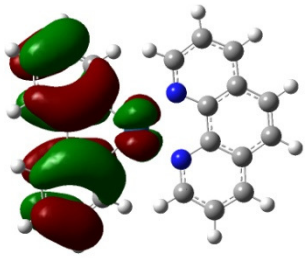

HOMO

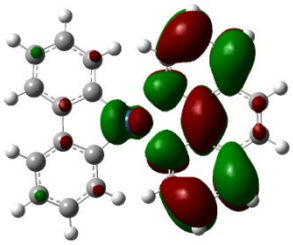

LUMO

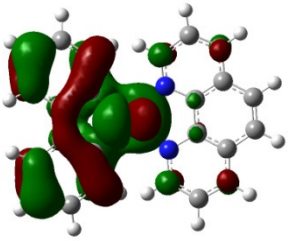

H-1

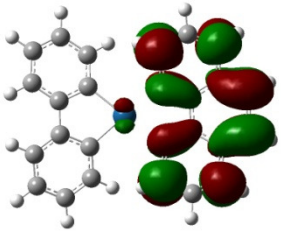

L+1

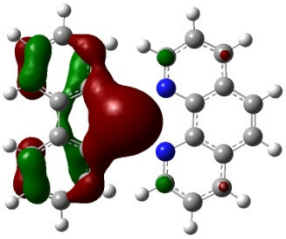

H-2

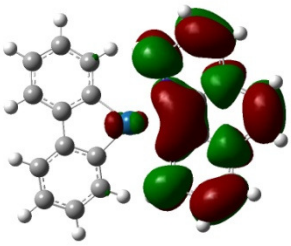

L+2

Figure 2.11 Frontior orbitals of Pt(bph)(phen)

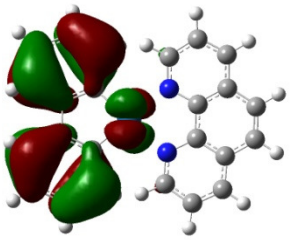

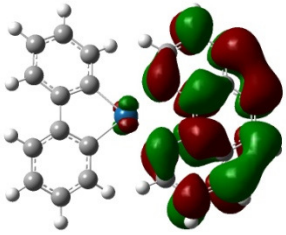

H-3 L+3

Figure 2.11 Molecular orbitals of Pt(bph)(phen) (continued)

Table 2.7 Orbital populations of Pt(bph)(phen) from calculations

	Energy level (eV)	Pt%	Bph%	Phen%
LUMO+5	0.09	103	1	-3
LUMO+4	-0.24	7	92	2
LUMO+3	-0.7	1	0	99
LUMO+2	-1.36	2	2	97
LUMO+1	-2.59	1	1	99
LUMO	-2.7	5	3	92
HOMO	-4.66	16	82	2
HOMO-1	-5.42	47	47	6
HOMO-2	-5.55	73	25	2
HOMO-3	-5.59	18	81	1
HOMO-4	-6.48	68	28	3
HOMO-5	-6.6	54	38	7

Table 2.8 Calculated singlet energy state transitions for Pt(bph)(phen)

ν(cm^{-1})	λ (nm)	f	Major orbital contributions	Nature of transition
18606	537	0.1373	H-2→LUMO (-36%),H-1→LUMO (46%)	MLCT Pt→phen
28718	348	0.0766	H-2→L+2 (40%), H-1→L+2 (-32%)	MLCT Pt,bph→phen
30679	325	0.0584	HOMO→L+4 (69%)	IL$\pi\rightarrow\pi^*$ bph
37810	264	0.1136	H-11→L+1 (51%)	IL$\pi\rightarrow\pi^*$ phen
39235	255	0.1618	H-11→LUMO (32%), H-10→L+1 (-15%),	IL$\pi\rightarrow\pi^*$ phen
39694	252	0.3026	H-3→L+4 (44%)	IL$\pi\rightarrow\pi^*$ bph
40582	246	0.2389	H-4→L+3 (21%), H-3→L+4 (13%)	
40742	245	0.0559	H-4→L+3 (70%)	MLCT Pt→phen

2.4.4 Comparison of UV/Vis spectra with calculations

Figure 2.12 shows an overlay of the experimental and calculated UV/Vis absorption spectra of [Pt(bph)(bpy)] and [Pt(bph)(phen)]. The comparison of experimental and calculations maxima are listed in Table 2.9. The MLCT band at 440 nm is from platinum to bpy or phen, not from platinum to bph, since bpy and phen have lower unoccupied orbitals than bph. This is in agreement with Pt(bpy)(en) and Pt(bpy)Cl_2, which have MLCT Pt→bpy transitions located at 447 and 394 nm.[21] On the other hand, complexes like Pt(bph)L (L= $(C_2H_5)_2S$, py, CH_3CN, en, CO), have metal-to-ligand transitions from platinum to bph located in 300~380 nm region.[6] In this case L has higher unoccupied orbitals than bph. Absorptions in the region of 300 nm are an over lay of multiple sources of transitions. According to the calculations, MLCT, IL and even LL have contributions to the bands in this region.

Table 2.9 Assignments of absorption spectra

complex	experimental		calculations	
	Absorption	Assignment	Transition	Assignment
Pt(bph)(bpy)	260	LC	251	IL$\pi\rightarrow\pi^*$ bph
	292		274	IL$\pi\rightarrow\pi^*$ bpy
	312			
	440	MLCT	559	MLCT Pt→bpy
Pt(bph)(phen)	260	LC	252	IL$\pi\rightarrow\pi^*$ bph
	314		255	IL$\pi\rightarrow\pi^*$ phen
	358			
	442	MLCT	537	MLCT Pt→phen

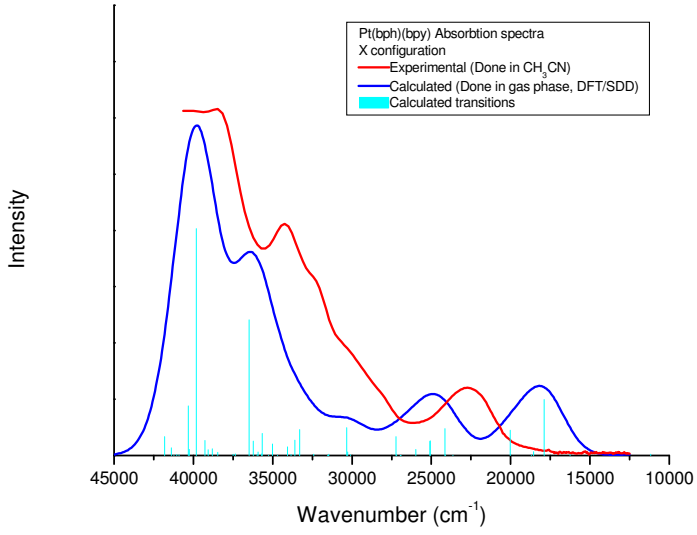

Figure 2.12(a) Experimental and calculated electronic absorption spectra of Pt(bph)(bpy)

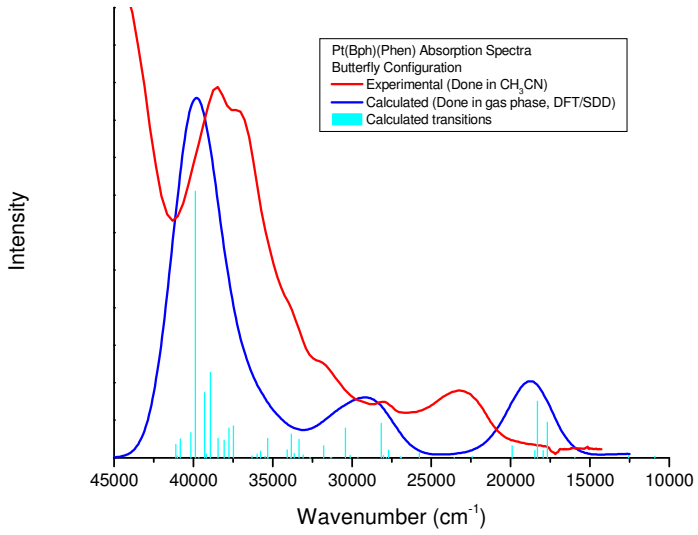

Figure 2.12(b) Experimental and calculated electronic absorption spectra of Pt(bph)(phen)

2.4.5 Emission

In the emission spectrum of Pt(bph)(bpy), λ_{max} is located at 488 nm (20491 cm^{-1}) at 77K with highly resolved vibronic structure. It is a ligand centered transition ^{3}LC bpy→G.S.[21] This is quite similar to Pt(bpy)(en), $Pt(bpy)_2^{2+}$, etc. The origin of Pt(bph)(phen) luminesence is more difficult to determine than for Pt(bph)(bpy). One reason is phen has much more complicated orbitals than bpy which makes the excited state ^{3}MLCT, ^{3}LC and ^{3}LF more complicated. The λ_{max} of emission is 586 nm (17065 cm^{-1}) and the emission curve is a broad band without vibronic structure unlike a ligand centered transition. The possible transitions are ^{3}MLCT and ^{3}LF. Due to the lack of information from TDDFT calculations for triplet states, the lowest excited state is still unclear. The emission maximum, λ_{max}, does not change much with various solvent as shown in Fig 2.13 and behaves more like a ^{3}LF state.[21]

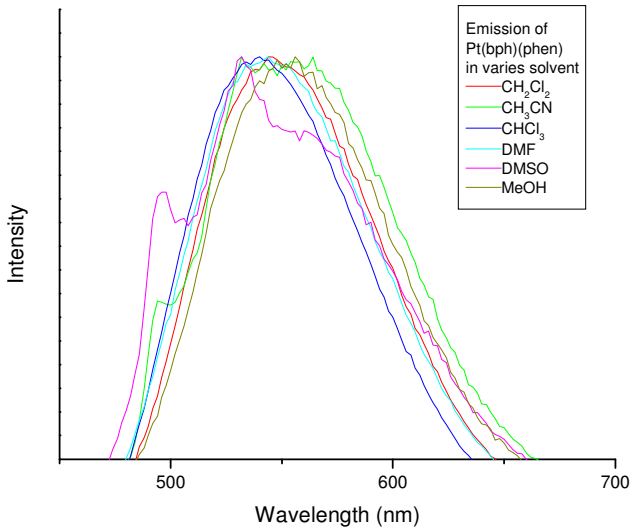

Figure 2.13 Emission maximum of Pt(bph)(phen) in different solvents

2.5 Conclusion

Pt(bph)(bpy) and Pt(bph)(phen) were synthesized and charcterized. Crystallography and CD shows complexes have two types of configuration X and B in the solid state as well as in solution. TDDFT calculation show the LUMO orbital for both systems is located on the diimine ligand instead of bph. Luminesence of complexes have different mechanisms, ^{3}LC and ^{3}LF.

CHAPTER 3

STRUCTURE, ELECTRONIC, AND PHOTOPHYSICAL PROPERTIES OF PLATINUM(II) BIPHENYL COMPLEXES CONTAINING 1,10-PHENANTHROLINE DERIVATIVES

3.1 Introduction

Platinum(II) phenanthroline complexes have been studied for decades.[1-4] Compared with bipyridine, phenanthroline has much more complicated π orbitals. This makes the absorption and emission spectra of the complexes harder to interpret[10]. The possible excited state of the emission can be metal-to-ligand charge transfer (MLCT), ligand centered (LC), ligand field (LF) and ligand-to-ligand charge transfer (LLCT).[6]

Here we report the synthesis, characterization and photoluminescence studies of a series of Pt(bph)(phen) complexes with different substituents attached to the phenanthroline ligand.

3.2 Experimental section

3.2.1 General procedures and chemicals

All syntheses were performed under a dry and oxygen-free nitrogen atmosphere using standard Schlenk-tube techniques. Anhydrous diethyl ether (99.7%) and anhydrous tetrahydrofuran (THF) (99.9%) were used as received from Aldrich. The other solvents methylene chloride, hexanes, butyronitrile, etc. were used without further purification. Potassium tetrachloroplatinate(II) was purchased from Alfa Aesar. All the ligands were purchased commercially without further purification. Diethyl sulfide and n-butyl lithium were purchased from Aldrich. 2,2'-Dibromobiphenyl,[25] 2,2'-dilithiobiphenyl,[26] and $Pt((C_2H_5)_2S)_2Cl_2$[27] were prepared by published procedures.

3.2.2 Instrumentation and physical measurements.

UV-Vis spectra were obtained using a Hewlett-Packard model 8452A diode array spectrophotometer interfaced with an OLIS software program. The IR spectra were acquired using a Nicolet Avatar 360 FT-IR spectrophotometer. Proton NMR spectra were obtained using a Varian Inova 400 FT-NMR spectrometer. Elemental (C, H, & N) analysis was performed by MHW Laboratories. An EG&G PAR model 263A potentiostat/galvanostat was used to obtain the cyclic voltammograms. The measurements were carried out in a typical H-cell using a platinum disk working electrode, a platinum wire counter electrode, and a Ag/AgCl reference electrode in acetonitrile. The supporting electrolyte used was 0.1M tetrabutylammonium hexafluorophosphate (TBAH). Ferrocene was added as the electrochemical reference.

Corrected emission spectra were collected using a Spex Tau3 Fluorometer. The excited state lifetimes were determined by exciting samples at 355 nm using an OPOTEK optical parametric oscillator pumped by a frequency tripled Continuum Surlite Nd:YAG laser. The emission curve-fittings were performed using the Origin 6.1 program by a non-the linear curve-fitting mode.

3.2.3 Calculations

Gaussian ’03 (Rev. B.03) software for UNIX was used for calculations. The molecules were optimized using Becke's three-parameter hybrid functional B3LYP[22] with the local term of Vosko, Wilk, and Nassiar. The basis set SDD[23] was chosen for all atoms and the geometry optimizations were all run in the gas phase. TDDFT[24] calculations were employed to produce a number of singlet excited states in the gas phase based on the optimized geometry. All vibrational analyses revealed no negative frequencies and were run in the gas phase only.

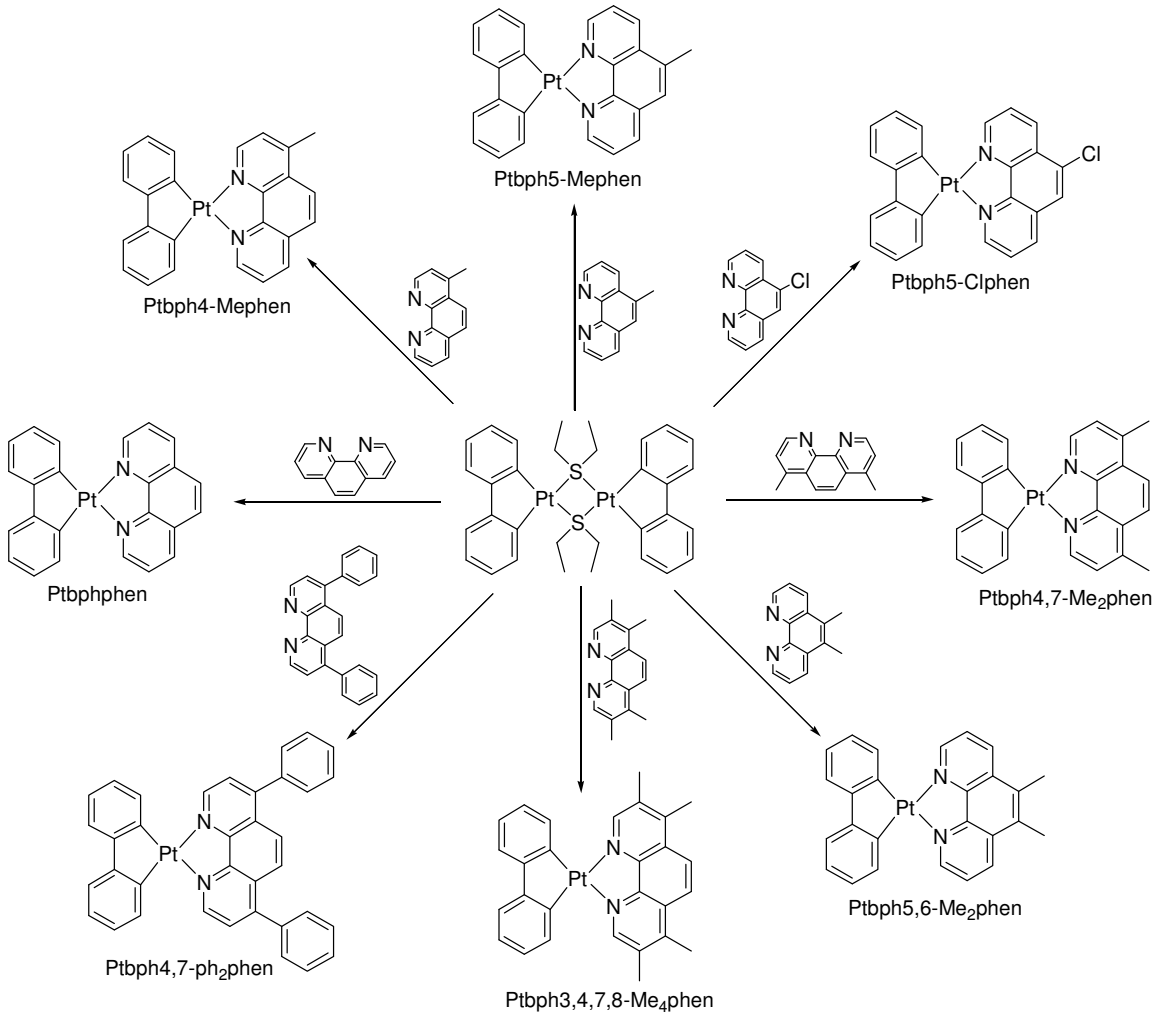

Figure 3.1 Preparation of complexes

3.2.4 Preparation of complexes

Pt(bph)(4-Mephen)

A solution of 4-methyl-1,10-phenanthroline (49 mg, 0.25 mmol) in methylene chloride (10 mL) was added dropwise to a solution of $[Pt(bph)(C_2H_5)_2S]_2$ (100 mg, 0.114 mmole) in methylene chloride (20 mL) under continuous stirring. The reaction mixture was stirred at room temperature for half hour and then rotary-evaporated to about 10 mL. The purple crystals were isolated and washed with ether. Anal. Calcd. for $C_{25}H_{18}N_2Pt$: C, 55.45; H, 3.35; N, 5.18. Found:

C, 55.34; H, 3.41; N, 5.26. IR (KBr pellet): 3030, 2924, 1629, 1411, 832, 738, 715 cm^{-1}. ^{1}H-NMR (CD_2Cl_2): δ ppm 9.91 (d, 1H, *J* = 5.3 Hz), 9.74 (d, 1H, *J* = 5.3 Hz), 8.69 (d, 1H, *J* = 8.3 Hz), 8.19 (d, 1H, *J* = 9.2 Hz), 8.02 (d, 1H, *J* = 9.2 Hz), 7.98 (dd, 1H, *J* = 8.3, 5.4 Hz), 7.82 (d, 1H, *J* = 5.4 Hz), 7.54 (m, 2H), 7.33 (dd, 2H, *J* = 6.8, 2.0 Hz), 6.98 (td, 2H, *J* = 6.8, 2.0 Hz), 6.94 (td, 2H, *J* = 6.8, 2.0 Hz), 2.86 (s, 3H).

Pt(bph)(5-Mephen)

A solution of 5-methyl-1,10-phenanthroline (49 mg, 0.25 mmol) in methylene chloride (10 mL) was added dropwise to a solution of $[Pt(bph)(C_2H_5)_2S]_2$ (100 mg, 0.114 mmole) in methylene chloride (20 mL) under continuous stirring. The red reaction mixture was stirred at room temperature for half hour and then rotary-evaporated to about 10 mL. The deep red crystalline material was isolated and washed with ether. Anal. Calcd. for $C_{25}H_{18}N_2Pt$: C, 55.45; H, 3.35; N, 5.18. Found: C, 54.47; H, 3.61; N, 4.98. IR (KBr pellet): 3033, 2924, 1630, 1422, 876, 794, 745, 720 cm^{-1}. ^{1}H-NMR (CD_2Cl_2): δ ppm 9.91 (dd, 1H, *J* = 5.3, 1.2 Hz), 9.85 (dd, 1H, *J* = 5.3, 1.2 Hz), 8.80 (dd, 1H, *J* = 8.3, 1.2 Hz), 8.59 (dd, 1H, *J* = 8.3, 1.2 Hz), 8.02 (dd, 1H, *J* = 8.3, 5.4 Hz), 7.96 (dd, 1H, *J* = 8.3, 5.4 Hz), 7.96 (dd, 1H, *J* = 8.3, 5.4 Hz), 7.54 (m, 2H), 7.34 (m, 2H, *J* = 6.8 Hz), 6.96 (td, 4H, *J* = 6.8, 2.0 Hz), 2.88 (s, 3H).

Pt(bph)(4,7-Me_2phen)

A solution of 4,7-dimethyl-1,10-phenanthroline (52 mg, 0.25 mmol) in methylene chloride (10 mL) was added dropwise to a solution of $[Pt(bph)(C_2H_5)_2S]_2$ (100 mg, 0.114 mmole) in methylene chloride (20 mL) under continuous stirring. The orange reaction mixture was stirring at room temperature for half hour and then rotary-evaporated to about 10 mL. The orange crystalline material was isolated and washed with ether. Anal. Calcd. for $C_{26}H_{20}N_2Pt$: C, 56.21; H, 3.63; N, 5.04. Found: C, 56.40; H, 3.82; N, 5.25. IR (KBr pellet): 3038, 1423, 1034,

847, 746, 715 cm^{-1}. ^{1}H-NMR (CD_2Cl_2): δ ppm 9.75 (d, 2H, *J* = 5.3 Hz), 8.22 (s, 2H), 7.71 (d, 2H, *J* = 5.3 Hz), 7.54 (d, 2H, *J* = 6.8, 2.0 Hz), 7.33 (dd, 2H, *J* = 6.8, 2.0 Hz), 6.99 (td, 2H, *J* = 6.8, 2.0 Hz), 6.92 (td, 2H, *J* = 6.8, 2.0 Hz), 2.86 (s, 6H).

Pt(bph)(5,6-Me_2phen)

A solution of 5,6-dimethyl-1,10-phenanthroline (52 mg, 0.25 mmol) in methylene chloride (10 mL) was added dropwise to a solution of $[Pt(bph)(C_2H_5)_2S]_2$ (100 mg, 0.114 mmole) in methylene chloride (20 mL) under continuous stirring. The red reaction mixture was stirred at room temperature for half hour and then rotary-evaporated to about 10 mL. The red crystalline was isolated and washed with ether. Anal. Calcd. for$C_{26}H_{20}N_2Pt$: C, 56.21; H, 3.63; N, 5.04. Found: C, 55.99; H, 3.90; N, 4.96. IR (KBr pellet): 3046, 2924, 1610, 1416, 1383, 796, 736, 718 cm^{-1}. ^{1}H-NMR (CD_2Cl_2): δ ppm 9.87 (d, 2H, *J* = 5.3 Hz), 8.73 (d, 2H, *J* = 8.0 Hz), 7.91 (dd, 4H, *J* = 8.0, 5.3 Hz), 7.48 (d, 2H, *J* = 6.8 Hz), 7.37 (dd, 2H, *J* = 6.8, 2.0 Hz), 6.99 (td, 2H, *J* = 6.8, 2.0 Hz), 6.92 (td, 2H, *J* = 6.8, 2.0 Hz), 2.78 (s, 6H).

Pt(bph)(3,4,7,8-Me_4phen)

A solution of 3,4,7,8-Tetramethyl-1,10-phenanthroline (59 mg, 0.25 mmol) in methylene chloride (10 mL) was added dropwise to a solution of $[Pt(bph)(C_2H_5)_2S]_2$ (100 mg, 0.114 mmole) in methylene chloride (20 mL) under continuous stirring. The solution was stirred at room temperature for half hour and then rotary-evaporated to about 10 mL. The orange color product was isolated and washed by ether. Anal. Calcd. for $C_{28}H_{24}N_2Pt$: C, 57.63; H, 4.15; N, 4.80. Found: C, 57.31; H, 4.20; N, 4.66. IR (KBr pellet): 3041, 2959, 1521, 1423, 1380, 1015, 911, 808, 738, 715 cm^{-1}. ^{1}H-NMR (CD_2Cl_2): δ ppm 9.61 (s, 2H), 8.20 (s, 2H), 7.52 (dd, 2H, *J* = 6.9, 2.0 Hz), 7.33 (dd, 2H, *J* = 6.9, 2.0 Hz), 6.95 (m, 4H, *J* = 6.9, 2.0 Hz), 2.75 (s, 6H), 2.71(s, 6H).

Pt(bph)(4,7-ph$_2$phen)

A solution of 4,7-diphenyl-1,10-phenanthroline (83 mg, 0.25 mmol) in methylene chloride (10 mL) was added dropwise to a solution of $[Pt(bph)(C_2H_5)_2S]_2$ (100 mg, 0.114 mmole) in methylene chloride (20 mL) under continuous stirring. The solution was stirred at room temperature for half hour and then rotary-evaporated to about 10 mL. The red color product was isolated and washed with ether. Anal. Calcd. for $C_{36}H_{24}N_2Pt$: C, 63.62; H, 3.53; N, 4.12. Found: C, 64.03; H, 3.90; N, 4.36. IR (KBr pellet): 3038, 2976, 1431, 1018, 835, 761, 734, 707 cm^{-1}. ^{1}H-NMR (CD_2Cl_2): δ ppm 9.98 (d, 2H, *J* = 5.3 Hz), 8.08 (s, 2H), 7.95 (d, 2H, *J* = 5.3 Hz), 7.64 (m, 12H), 7.35 (dd, 2H, *J* = 6.8, 2.0 Hz), 6.92 (m, 4H, *J* = 6.8, 2.0 Hz).

Pt(bph)(5-Clphen)

A solution of 5-chloro-1,10-phenanthroline (54 mg, 0.25 mmol) in methylene chloride (10 mL) was added dropwise to a solution of $[Pt(bph)(C_2H_5)_2S]_2$ (100 mg, 0.114 mmole) in methylene chloride (20 mL) under continuous stirring. The solution was heated at reflux for half hour and then rotary-evaporated to about 5 mL and was dripped into 500 mL hexanes. A brown precipitate was isolated and washed with ether. Anal. Calcd. for $C_{24}H_{15}N_2PtCl$: C, 51.30; H, 2.69; N, 4.99. Found: C, 50.93; H, 2.73; N, 4.71. IR (KBr pellet): 3040, 1617, 1576, 1416, 1424, 961, 743, 715, 732 cm^{-1}. ^{1}H-NMR (CD_2Cl_2): δ ppm 9.96(d, 1H, *J* = 5.2 Hz), 9.89 (dd, 1H, *J* = 5.2 Hz), 9.03 (dd, 1H, *J* = 8.0, 1.2 Hz), 8.60 (dd, 1H, *J* = 8.0, 1.2 Hz), 8.17 (s, 1H), 8.08 (dd, 1H, *J* = 8.0, 5.2 Hz), 7.97 (dd, 1H, *J* = 8.0, 5.2 Hz), 7.48 (td, 2H, *J* = 6.9, 2.0 Hz), 7.39 (dd, 2H, *J* = 6.9, 2.0 Hz), 6.92 (m, 4H, *J* = 6.9, 2.0 Hz).

3.3 Results and discussion

3.3.1 Analysis of ^{1}H NMR

The ^{1}H NMR spectra of platinum biphenyl complexes are complicated due to multiple types of hydrogen atoms on the aromatic rings. The chemical shifts of hydrogen from the complexes are listed in Table 3.1 as well as from Pt(bph)(phen) and $[Pt(bph)SEt]_2$. Chemical shifts of hydrogen atoms from bph ligand rings are located at 7.5, 7.3 and 6.9 ppm with coupling constants 6.8 and 2.0 Hz. Those from phenanthroline derivative rings range from 9.9 to 7.6 ppm with coupling constants 8, 5.3 and 1.2 Hz. Figure 3.2 displays the assignments of different types of hydrogen atoms from bph and phen.

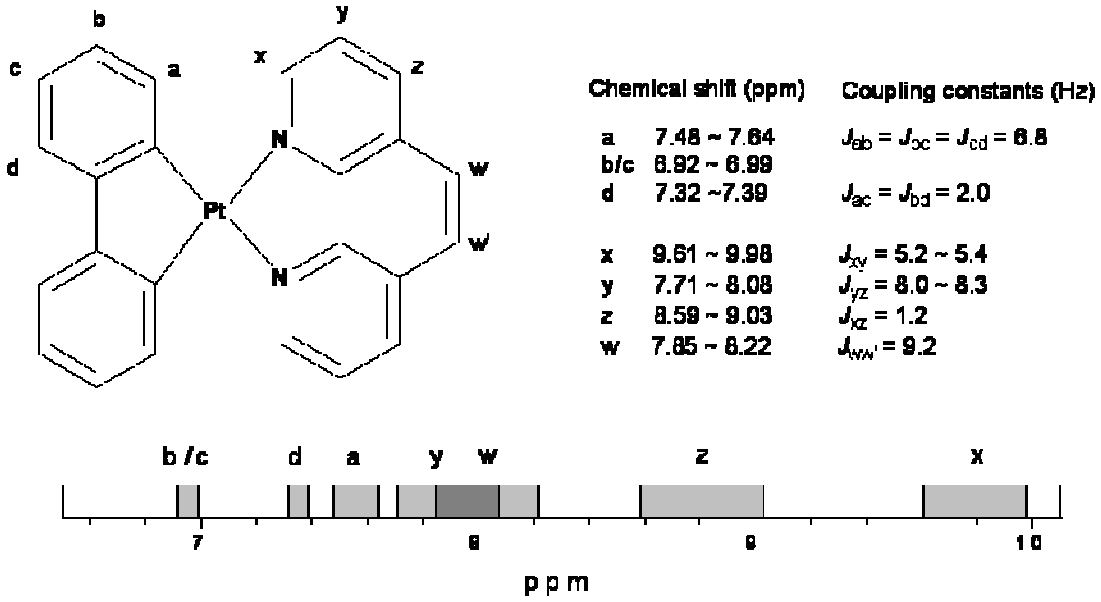

Figure 3.2 scheme for ^{1}H NMR assignments

Table 3.1 Chemical shifts and coupling constants of ^{1}H NMR

Complexes	phen	bph	others
$[Pt(bph)Set]_2$		7.29 (dd, 2H, *J* = 6.8, 2.0), 7.01 (dd, 2H, *J* = 6.8, 2.0), 6.90 (m, 4H, *J* = 6.8, 2.0).	3.83(q, 4H, *J* = 7.2), 1.76(t, 6H, *J* = 7.2).
Pt(bph)(phen)	9.93 (dd, 2H, *J* = 5.2, 1.2), 8.69 (dd, 2H, *J* = 8.0, 1.2), 8.02 (s, 2H) 8.00 (dd, 2H, *J* = 8.0, 5.2).	7.55 (dd, 2H, *J* = 6.8, 2.0), 7.34 (dd, 2H, *J* = 6.8, 2.0), 6.97 (m, 4H, *J* = 6.8, 2.0).	
Pt(bph)(5-Mephen)	9.91 (dd, 1H, *J* = 5.3, 1.2), 9.85 (dd, 1H, *J* = 5.3, 1.2), 8.80 (dd, 1H, *J* = 8.3, 1.2), 8.59 (dd, 1H, *J* = 8.3, 1.2), 8.02 (dd, 1H, *J* = 8.3, 5.4), 7.96 (dd, 1H, *J* = 8.3, 5.4), 7.85 (s, 1H).	7.54 (m, 2H), 7.34 (m, 2H, *J* = 6.8), 6.96 (td, 4H, *J* = 6.8, 2.0).	2.88 (s, 3H).
Pt(bph)(4-Mephen)	9.91 (d, 1H, *J* = 5.3), 9.74 (d, 1H, *J* = 5.3), 8.69 (d, 1H, *J* = 8.3), 8.19 (d, 1H, *J* = 9.2), 8.02 (d, 1H, *J* = 9.2), 7.98 (dd, 1H, *J* = 8.3, 5.4), 7.82 (d, 1H, *J* = 5.4).	7.54 (m, 2H), 7.33 (dd, 2H, *J* = 6.8, 2.0), 6.98 (td, 2H, *J* = 6.8, 2.0), 6.94 (td, 2H, *J* = 6.8, 2.0).	2.86 (s, 3H).
Pt(bph)(4,7-Me_2phen)	9.75 (d, 2H, *J* = 5.3), 8.22 (s, 2H), 7.71 (d, 2H, *J* = 5.3).	7.54 (dd, 2H, *J* = 6.8, 2.0), 7.33 (dd, 2H, *J* = 6.8, 2.0), 6.99 (td, 2H, *J* = 6.8, 2.0), 6.92 (td, 2H, *J* = 6.8, 2.0).	2.86 (s, 6H).

Table 3.1 Chemical shifts and coupling constants of ^{1}H NMR (continued)

Complexes	phen	bph	others
Pt(bph)(5,6-Me_2phen)	9.87 (d, 2H, *J* = 5.3), 8.73 (d, 2H, *J* = 8.0), 7.91 (dd, 2H, *J* = 8.0, 5.3).	7.48 (d, 2H, *J* = 6.8), 7.37 (dd, 2H, *J* = 6.8, 2.0), 6.99 (td, 2H, *J* = 6.8, 2.0), 6.92 (td, 2H, *J* = 6.8, 2.0).	2.78 (s, 6H)
Pt(bph)(3,4,7,8-Me_4phen)	9.61 (s, 2H), 8.20 (s, 2H).	7.52 (dd, 2H, *J* = 6.9, 2.0), 7.33 (dd, 2H, *J* = 6.9, 2.0), 6.95 (m, 4H, *J* = 6.9, 2.0),	2.73 (s, 6H), 2.69(s, 6H).
Pt(bph)(4,7-ph_2phen)	9.98 (d, 2H, *J* = 5.3), 8.08 (s, 2H), 7.95 (d, 2H, *J* = 5.3).	7.64 (m, 2H), 7.35 (dd, 2H, *J* = 6.8, 2.0), 6.92 (m, 4H, *J* = 6.8, 2.0)	7.64 (m, 10H)
Pt(bph)(5-Clphen)	9.96 (d, 1H, *J* = 5.2), 9.89 (d, 1H, *J* = 5.2), 9.03 (dd, 1H, *J* = 8.0, 1.2), 8.60 (dd, 1H, *J* = 8.0, 1.2), 8.17 (s, 1H), 8.08 (dd, 1H, *J* = 8.0, 5.2), 7.97 (dd, 2H, *J* = 8.0, 5.2),	7.48 (td, 2H, *J* = 6.9, 2.0), 7.39 (dd, 2H, *J* = 6.9, 2.0), 6.92 (m, 4H, *J* = 6.9, 2.0).	

Figure 3.3 shows the ^{1}H NMR of Pt(bph)(phen) and Pt(bph)(5-Clphen). There are satellite peaks at 7.4 ppm and unresolved satellite peaks at 9.9 ppm. The intensity of the satellite peaks is about one fourth to one fifth of the center peaks. The signals at 7.4 and 9.9 ppm are due to hydrogen atoms located at a and x positions, respectively. The origin of the satellite peaks is the splitting of the proton signal by the ^{195}Pt isotope, which has a nuclear spin of ½ and a natural abundance of 33.8%. The coupling constant *J* (Pt, H) is about 48 Hz. This is shown by the inset in Figure 3.4.

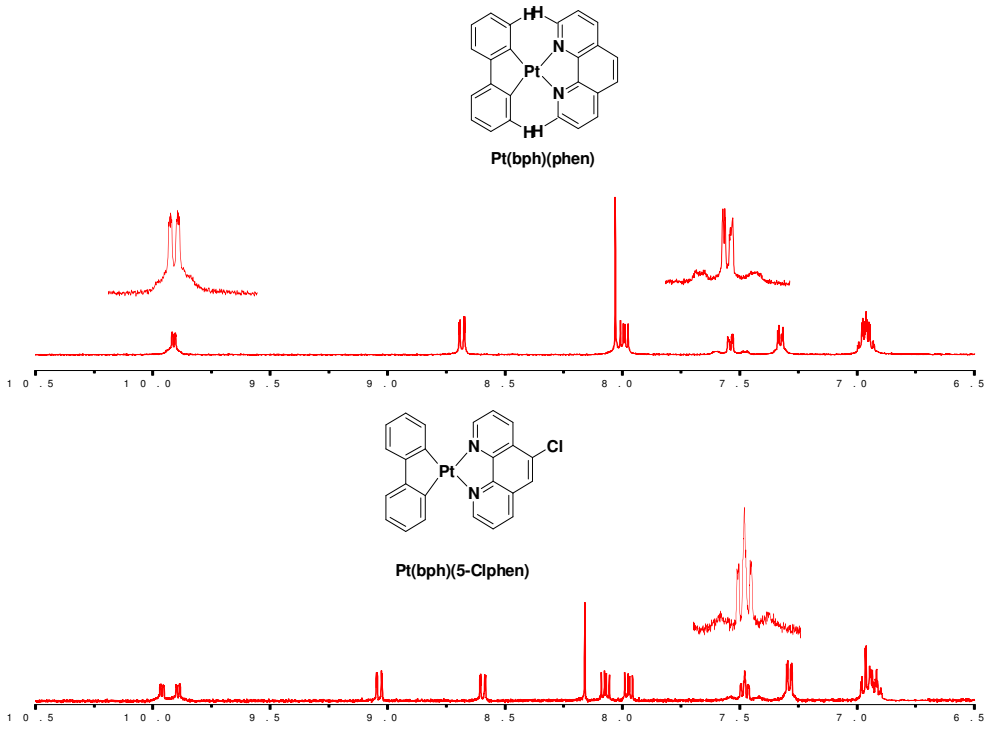

Figure 3.3 ^{1}H NMR of Pt(bph)(phen) and Pt(bph)(5-Clphen)

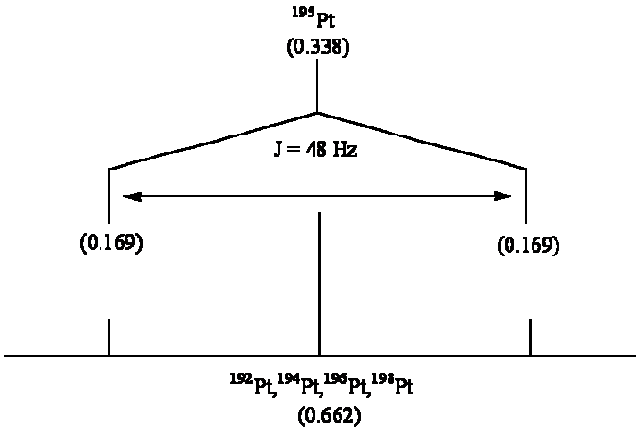

isotope	Nuclear spin	Isotope mole fraction
^{192}Pt	0	0.00782
^{194}Pt	0	0.32967
^{195}Pt	1/2	0.33832
^{196}Pt	0	0.25242
^{198}Pt	0	0.07163

Figure 3.4 Scheme for ^{195}Pt- ^{1}H coupling

3.3.2 X-Ray crystallographic data collection

The crystals were affixed to a nylon cryoloop using oil (Paratone-n, Exxon) and mounted in the cold stream of a Bruker Kappa-Apex-II[28] area-detector diffractometer. The temperature at the crystal was maintained at 150 K using a Cryostream 700EX Cooler (Oxford Cryosystems). The unit cell was determined from the setting angles of 383 reflections collected in 36 frames of data for Pt(bph)(4,7-Me_2phen), 250 reflections for Pt(bph)(5-Mephen), 151 reflections for Pt(bph)(4,7-ph_2phen), 108 reflections for Pt(bph)(4-Mephen) and 1037 reflections collected in 100 frames for Pt(bph)(5,6-Me_2phen). Data were measured with a redundancy of 7.9 for Pt(bph)(4,7-Me_2phen), 7.1 for Pt(bph)(5-Mephen), 6.45 for Pt(bph)(4,7-ph_2phen), 9.2 for Pt(bph)(4-Mephen) and 5.5 for Pt(bph)(5,6-Me_2phen) using a CCD detector at a distance of 50 mm from the crystal with a combination of phi and omega scans. A scan width of 0.5 degrees and time of 10 seconds was employed along with graphite mono-chromated molybdenum Kα radiation (λ= 0.71073 Å) that was collimated to a 0.6mm diameter. Data collection, reduction, structure solution, and refinement were performed using the Bruker Apex2 suite (v2.0-2). All available reflections to $2\theta_{max}$ = 52° (50° for Pt(bph)(4,7-Me_2phen)) were harvested (34568 reflections, 3356 unique for Pt(bph)(4,7-Me_2phen), 35940 reflections, 50744 reflections, 7009 unique for Pt(bph)(5-Mephen), 4979 unique for Pt(bph)(4,7-ph_2phen), 37727 reflections, 3712 unique for Pt(bph)(5,6-Me_2phen)and 34745 reflections, 3559 unique for Pt(bph)(4-Mephen)) and corrected for Lorentz and polarization factors with Bruker SAINT (v6.45).[28] Reflections were then corrected for absorption (numerical correction interframe scaling, and other systematic errors with SADABS 2004/1[28] (combined transmission and other correction factors min./max. = 0.1854/0.4862 for Pt(bph)(4,7-Me_2phen), 0.4329/0.8585 for Pt(bph)(5-Mephen), 0.5390/0.7144 for Pt(bph)(4,7-ph_2phen), 0.2145/0.5243 for Pt(bph)(5,6-Me_2phen) and 0.4479/0.6474 for

Pt(bph)(4-Mephen)). The structure was solved (direct methods) and refined (full-matrix least-squares against F^2) with the Bruker SHELXTL package (v6.14-1).[28] All non-hydrogen atoms were refined using anisotropic thermal parameters. All hydrogen atoms were included at idealized positions; hydrogen atoms were not refined. The compound Pt(bph)(4,7-Me_4phen) sits on a general position in the monoclinic space group $P2_1/n$, Pt(bph)(4,7-ph_2phen) in the triclinic space group P-1, Pt(bph)(5-Mephen) in the orthorhombic space group $Pca2_1$, Pt(bph)(5,6-Me_2phen) in the monoclinic space group $P2_1/c$ and Pt(bph)(4-Mephen) in the orthorhombic space group $P2_1cn$. Selected bond distances and angles are provided in Tables 3.2~3.6. Figure 3.5~3.14 show the ORTEP and unit cell pictures of these crystals.

Table 3.2 Crystal data for Pt(bph)(4,7-ph_2phen)

Empirical formula	$C_{36}H_{24}N_2Pt_1$
Formula weight	679.66
Temperature	150 K
Wavelength	0.71073 Å
Crystal system	Triclinic
Space group	*P*-1
Unit cell dimensions	a = 10.671 Å b = 11.235 Å c = 11.862 Å α = 90.41° β = 108.80° γ = 108.23°
Volume	1269.5 $Å^3$
Z	2
Calculated density	1.778 g/cm^3
Absorption coefficient	5.556 mm^{-1}
F(000)	664
Crystal size	0.18 x 0.16 x 0.09 mm
Crystal habit	Plate
Crystal color	Lustrous Intense Red
θ range for data collection	3.29^o to 26.00^o
Limiting indices	$-13 \leq h \leq 13$ $-13 \leq k \leq 13$ $-14 \leq l \leq 14$
Reflections collected / unique	35940 / 4979 [R(int) = 0.0716]
Completeness to θ = 26.00	99.8 %
Refinement method	Full-matrix least-squares on F^2
Data / restraints / parameters	4979 / 0 / 352
Refinement threshold	I>2σ(I)
Data > threshold	4365
Goodness-of-fit on F^2	1.037
Final R indices [I>2σ(I)]	R1 = 0.0267, wR2 = 0.0492
R indices (all data)	R1 = 0.0353, wR2 = 0.0519
Largest diff. peak and hole	0.822 and -0.957 e^- $Å^{-3}$

Table 3.3 Crystal data for Pt(bph)(4,7-Me_2phen)

Empirical formula	$C_{26}H_{20}N_2Pt_1$
Formula weight	555.53
Temperature	150 K
Wavelength	0.71073 Å
Crystal system	Monoclinic
Space group	$P2_1/n$
Unit cell dimensions	a = 7.5788(3) Å b = 17.5685(6) Å c = 14.6221(5) Å α = 90° β = 98.1480(10)° γ = 90°
Volume	1927.25(12) $Å^3$
Z	4
Calculated density	1.915 g/cm^3
Absorption coefficient	7.296 mm^{-1}
F(000)	1072
Crystal size	0.38 x 0.24 x 0.14 mm
Crystal habit	Block
Crystal color	Lustrous Orange
θ range for data collection	3.23° to 25.00°
Limiting indices	-8 ≤ h ≤ 8 -20 ≤ k ≤ 20 -17 ≤ l ≤ 16
Reflections collected / unique	34568 / 3356 [R(int) = 0.0235]
Completeness to θ = 25.00	99 %
Refinement method	Full-matrix least-squares on F^2
Data / restraints / parameters	3356 / 0 / 264
Refinement threshold	I>2σ(I)
Data > threshold	3084
Goodness-of-fit on F^2	1.079
Final R indices [I>2σ(I)]	R1 = 0.0148, wR2 = 0.0367
R indices (all data)	R1 = 0.0175, wR2 = 0.0377
Largest diff. peak and hole	0.990 and -0.234 $e^- Å^{-3}$

Table 3.4 Crystal data for Pt(bph)(5,6-Me_2phen)

Empirical formula	$C_{34}H_{26}N_2Pt_1$
Formula weight	657.17
Temperature	150 K
Wavelength	0.71073 Å
Crystal system	Monoclinic
Space group	$P2_1/c$
Unit cell dimensions	a = 13.7203(8) Å b = 7.2507(4) Å c = 19.9177(11) Å α = 90° β = 106.855(3)° γ = 90°
Volume	1896.33(18) $Å^3$
Z	4
Calculated density	1.946 g/cm^3
Absorption coefficient	7.414 mm^{-1}
F(000)	1072
Crystal size	0.30 x 0.30x 0.10 mm
Crystal habit	Hexagonal Plate
Crystal color	Translucent Light Red
θ range for data collection	1.55° to 26.00°
Limiting indices	-16≤ h ≤ 16 -8 ≤ k ≤ 8 -23 ≤ l ≤ 24
Reflections collected / unique	37727 / 3712 [R(int) = 0.0428]
Completeness to θ = 26.00	100 %
Refinement method	Full-matrix least-squares on F^2
Data / restraints / parameters	3712 / 0 / 264
Refinement threshold	I>2σ(I)
Data > threshold	3126
Goodness-of-fit on F^2	1.222
Final R indices [I>2σ(I)]	R1 = 0.0281, wR2 = 0.0613
R indices (all data)	R1 = 0.0419, wR2 = 0.0721
Largest diff. peak and hole	2.857 and -1.077 $e^- Å^{-3}$

Table 3.5 Crystal data for Pt(bph)(3,4,7,8-Me_4phen)

Empirical formula	$C_{28}H_{24}N_2Pt_1$
Formula weight	583.58
Temperature	150 K
Wavelength	0.71073 Å
Crystal system	Orthorhombic
Space group	$P2_1cn$
Unit cell dimensions	a = 7.1347(4) Å b = 12.9045(8) Å c = 22.5817(15) Å α = 90° β = 90° γ = 90°
Volume	2079.1(2) $Å^3$
Z	4
Calculated density	1.864 g/cm^3
Absorption coefficient	6.768 mm^{-1}
F(000)	1136
Crystal size	0.20 x 0.16 x 0.08 mm
Crystal habit	Hexagonal Plate
Crystal color	Translucent Light Red
θ range for data collection	2.40° to 25.99°
Limiting indices	$-7 \leq h \leq 8$ $-15 \leq k \leq 15$ $-27 \leq l \leq 27$
Reflections collected / unique	34745 / 3559 [R(int) = 0.1008]
Completeness to θ = 26.00	99.9 %
Refinement method	Full-matrix least-squares on F^2
Data / restraints / parameters	3559 / 1 / 284
Refinement threshold	I>2σ(I)
Data > threshold	2884
Goodness-of-fit on F^2	1.040
Final R indices [I>2σ(I)]	R1 = 0.0309, wR2 = 0.0671
R indices (all data)	R1 = 0.0410, wR2 = 0.0714
Largest diff. peak and hole	0.632 and -1.263 $e^- Å^{-3}$

Table 3.6 Crystal data for Pt(bph)(5-Mephen)

Empirical formula	$C_{25}H_{18}N_2Pt_1$
Formula weight	541.50
Temperature	150 K
Wavelength	0.71073 Å
Crystal system	Orthorhombic
Space group	$Pca2_1$
Unit cell dimensions	a = 17.1532(8) Å b = 10.2887(5) Å c = 20.6417(9) Å α = 90° β = 90° γ = 90°
Volume	3642.9(3)Å^3
Z	8
Calculated density	1.989 g/cm^3
Absorption coefficient	7.718 mm^{-1}
F(000)	2096
Crystal size	0.17 x 0.14 x 0.02 mm
Crystal habit	Plate
Crystal color	Clear Light Red
θ range for data collection	3.25° to 26.00°
Limiting indices	-21 ≤ h ≤ 21 -12 ≤ k ≤ 12 -25 ≤ l ≤ 25
Reflections collected / unique	50744 / 7009 [R(int) = 0.0582]
Completeness to θ = 26.00	99.7 %
Refinement method	Full-matrix least-squares on F^2
Data / restraints / parameters	7009 / 1 / 511
Refinement threshold	I>2σ(I)
Data > threshold	6231
Goodness-of-fit on F^2	1.025
Final R indices [I>2σ(I)]	R1 = 0.0283, wR2 = 0.0516
R indices (all data)	R1 = 0.0378, wR2 = 0.0545
Largest diff. peak and hole	0.984 and -0.852 e$^-$ Å^{-3}

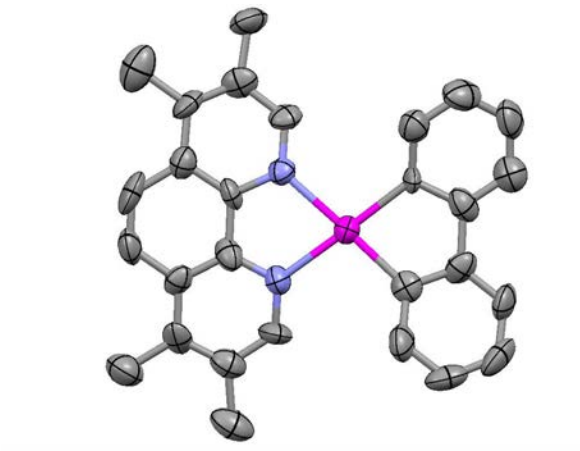

Figure 3.5 ORTEP diagram of Pt(bph)(3,4,7,8-Me_4phen)

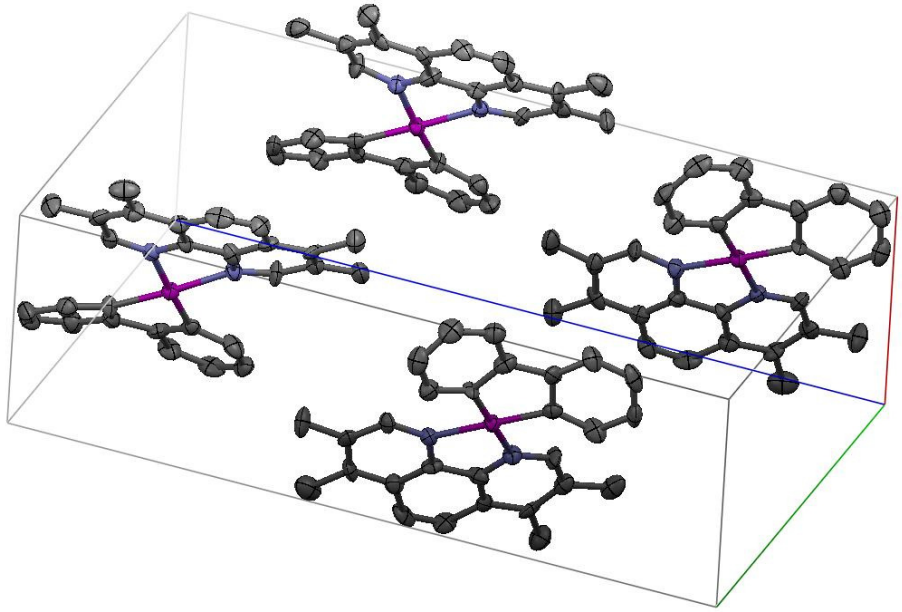

Figure 3.6 Unit Cell of Pt(bph)(3,4,7,8-Me_4phen)

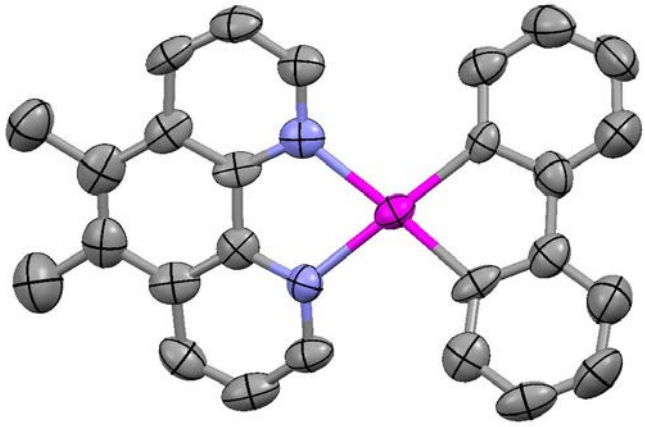

Figure 3.7 ORTEP diagram of Pt(bph)(5,6-Me_2phen)

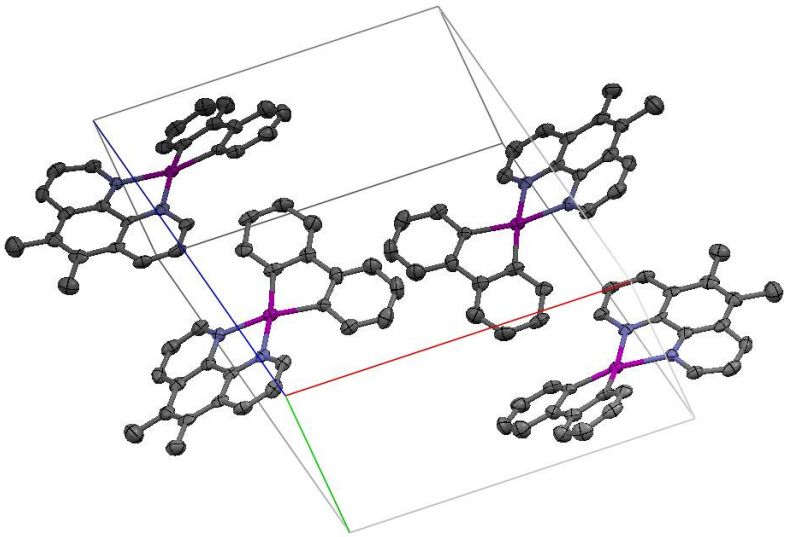

Figure 3.8 Unit cell of Pt(bph)(5,6-Me_2phen)

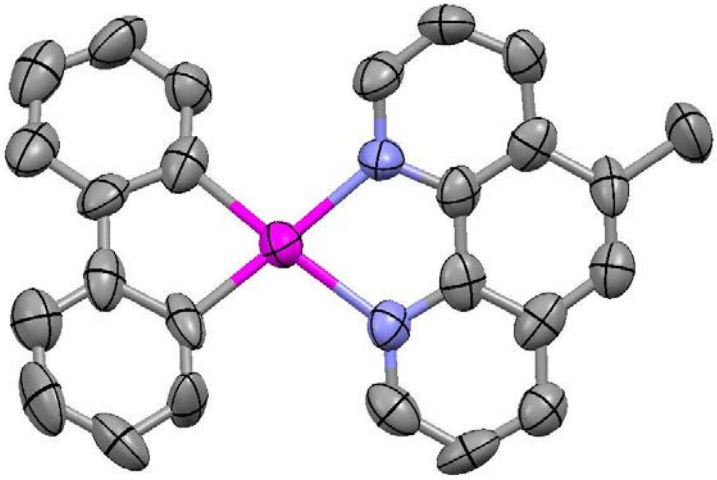

Figure 3.9 ORTEP diagram of Pt(bph)(5-Mephen)

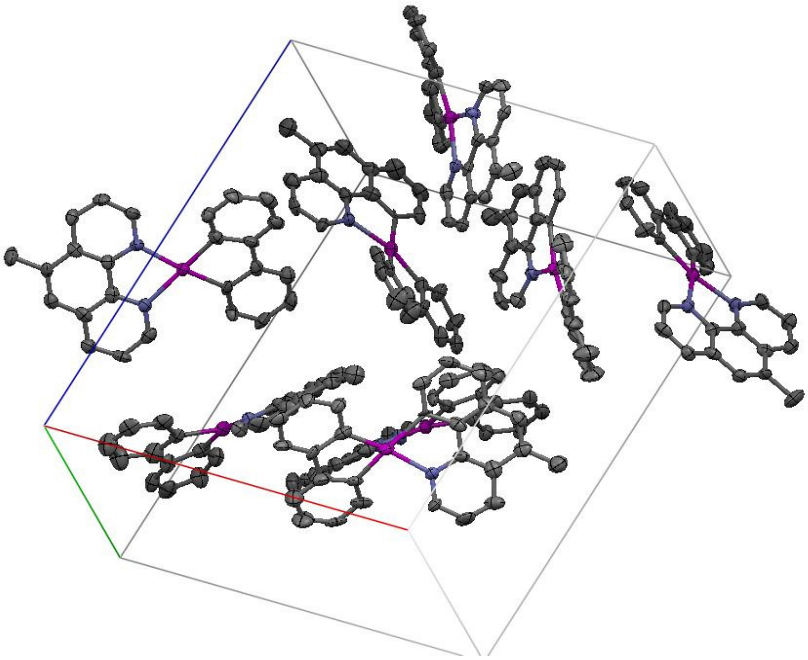

Figure 3.10 Unit cell of Pt(bph)(5,6-Me_2phen)

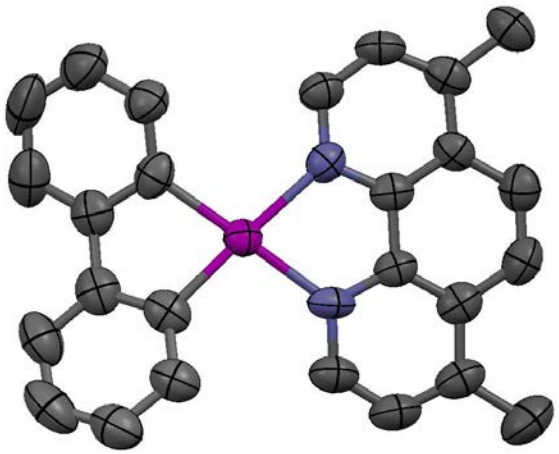

Figure 3.11 ORTEP diagram of Pt(bph)(4,7-Me_2phen)

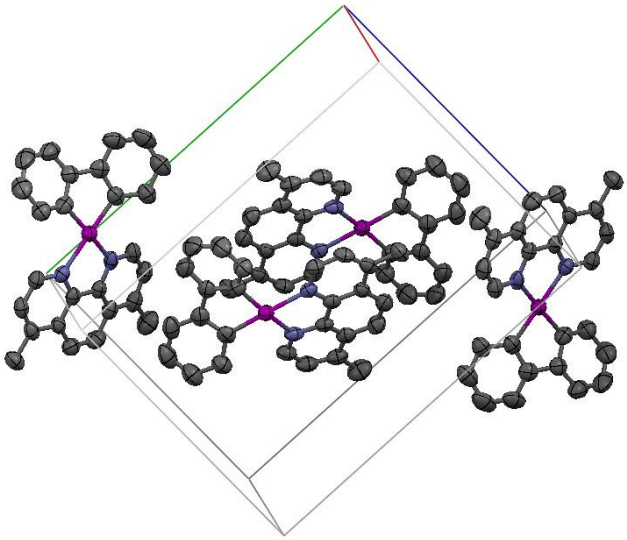

Figure 3.12 Unit cell of Pt(bph)(4,7-Me_2phen)

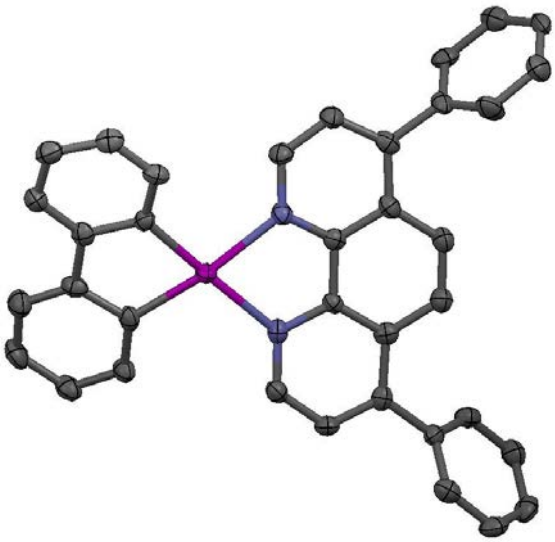

Figure 3.13 ORTEP diagram of Pt(bph)(4,7-ph_2phen)

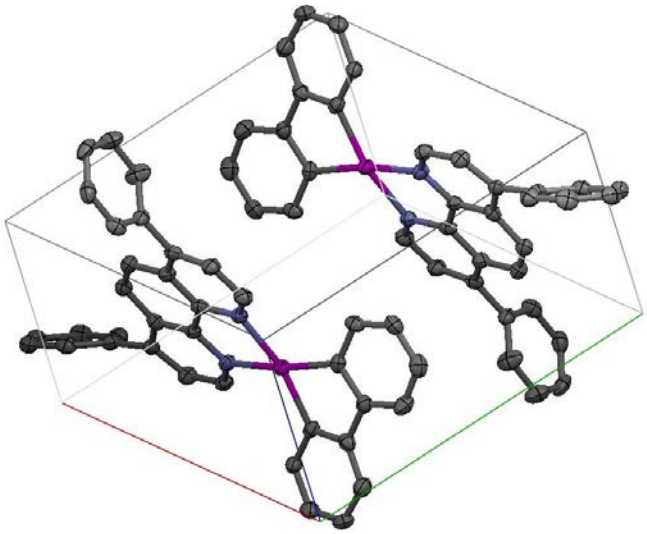

Figure 3.14 Unit cell of Pt(bph)(4,7-ph_2phen)

Table 3.7 selected bond length and bond angle

	Pt(bph)(3,4,7,8-Me_4phen)	Pt(bph)(4,7-Me_2phen)	Pt(bph)(5,6-Me_2phen)	Pt(bph)(4,7-ph_2phen)	Pt(bph)(5-Mephen)
Bond lengths(Å)					
Pt – C	2.015	2.006	2.015	2.015	2.036
Pt – C	2.013	2.021	2.011	2.014	2.055
Pt – N	2.120	2.088	2.124	2.133	2.169
Pt – N	2.136	2.134	2.122	2.114	2.112
Bond angles(deg)					
C – Pt – C	80.2	79.9	80.1	80.5	81.3
N – Pt – N	76.8	77.4	76.9	77.2	76.2
C – Pt – N	101.3	100.1	103.4	104.1	107.8
C – Pt – N	101.5	102.3	102.5	101.1	97.9
Dihedral (deg)					
C-C-N-N	1.86	6.48	20.35	21.01	19.07
Configuration	B	B	X	X	X

Crystals of Pt(bph)(3,4,7,8-Me_4phen), Pt(bph)(4,7-Me_2phen), Pt(bph)(5,6-Me_2phen), Pt(bph)(4,7-ph_2phen) and Pt(bph)(5-Mephen) were obtained by slow evaporation of saturated methylene chloride solutions. Selected bond distances and angles are given in Table 3.7. Bond lengths of platinum to carbon were between 2.006~2.055 Å and bond lengths of platinum to nitrogen were between 2.088~2.169 Å, which were normal compared to those of similar complexes.[31-33, 39-40] Bond angles of C – Pt – C varied between 79.9 to 81.3 deg. N – Pt – N angles were 76.2 to 77.4 deg.

In Pt(bph)(5,6-Me_2phen), Pt(bph)(4,7-ph_2phen) and Pt(bph)(5-Mephen), the coordination spheres of platinum metal center were twisted to give X configurations, shown in Figure 3.8, 3.10, 3.14. The C-C-N-N torsion angles were 20.19, 21.01 and 22.40 deg respectively. In Pt(bph)(3,4,7,8-Me_4phen) and Pt(bph)(4,7-Me_2phen) the coordination spheres of platinum metal center were planar. The C-C-N-N torsion (dihedral) angles were less than 7 deg. The bph and phen ligands wings were slightly bent over in opposite directions, which gave a butterfly-like configuration, shown in Figure 3.6 and 3.12. Unlike Pt(bph)(phen), no Pt–Pt interactions in the solid state are observed in all five crystal lattice. The shortest Pt-Pt distance is over 6 Å which is to long for any Pt-Pt interactions in the solid state.

3.3.3 Circular dichroism (CD) spectra and the X/B configurations

Among the eight platinum biphenyl phenanthroline complexes, including Pt(bph)(phen), six crystal structures were obtained. Three of them were in the X configuration and the other three were in the butterfly (B) configuration. The complexes with the X configuration, Pt(bph)(5-Mephen), Pt(bph)(4,7-ph_2phen) and Pt(bph)(5,6-Me_2phen) have C_2 symmetry if the substituents are not counted. The complexes with the B configuration, Pt(bph)(phen), Pt(bph)(4,7-Me_2phen) and Pt(bph)(3,4,7,8-Me_4phen) have C_s symmetry without counting the substituents. The complexes with C_2 symmetry are optically active and the complexes with C_s symmetry are not. But as shown in Figure 3.15, both types of complexes are optically active in solution. The C_2 complexes absorb one form of circularly polarized light and the C_s form rearranges in solution to give the X isomer that absorbs oppositely polarized light. Configurations of Pt(bph)(4-Mephen) and Pt(bph)(5-Clphen) are undetermined for the lack of single crystals but can be predicted from CD spectra. Figure 3.15 shows the CD spectra of

Pt(bph)(phen), Pt(bph)(5,6-Me_2phen), Pt(bph)(5-Clphen) and Pt(bph)(3,4,7,8-Me_4phen). As a tentative assignment, the CD spectrum of Pt(bph)(5-Clphen) belongs to the B group.

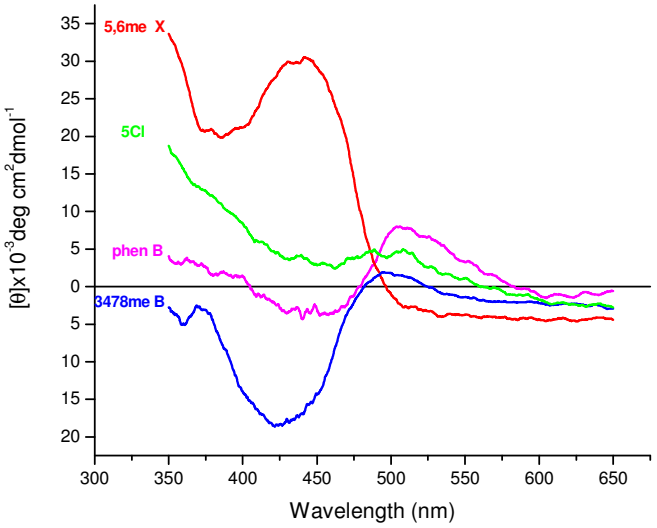

Figure 3.15 CD spectra of Pt(bph)(phen), Pt(bph)(5,6-Me_2phen), Pt(bph)(5-Clphen) and Pt(bph)(3,4,7,8-Me_4phen)

3.3.4 Optimized structures from DFT calculation

Calculated structures were optimized by DFT. The configurations of the molecules were initially set to X or B based on crystallographic structures or CD spectra. Selected bond lengths, bond angles and dihedral angles are listed in Table 3.8 with the values from crystallography in parentheses.

The bond lengths between platinum to carbon atom were between 2.033 to 2.016 Å. The bond lengths between platinum to nitrogen atom were between 2.126 to 2.164 Å. C-Pt-C and N-Pt-N bond angles were around 77° and 81°. In the coordination sphere the C-C-N-N dihedral angle was 23° for the X configuration and 0° for the B configuration. Optimized structures agree

with the crystal structures very well. The difference of bond lengths between optimized structures and crystal structures is ~ 0.02 Å.

In optimization structures, we used different basis sets, MP2/SDD, MP2/LanL2DZ and DFT/SDD, to check which configuration, X or B, had the lower energy. According to calculations, X always had the lower energy for both Pt(bph)(phen) and Pt(bph)(bpy). The reason for B configuration is likely due to intermolecular stacking in the solid state.

Table 3.8(a) Selected bond lengths (Å) from DFT optimized structures

	Pt-C	Pt-C	Pt-N	Pt-N
Pt(bph)(4-Mephen)	2.032	2.033	2.164	2.160
Pt(bph)(5-Mephen)	2.032 (2.036)	2.033 (2.055)	2.160 (2.169)	2.163 (2.112)
Pt(bph)(4,7-Me_2phen)	2.016 (2.006)	2.016 (2.021)	2.126 (2.088)	2.126 (2.134)
Pt(bph)(5,6-Me_2phen)	2.022 (2.015)	2.022 (2.011)	2.129 (2.124)	2.129 (2.122)
Pt(bph)(3,4,7,8-Me_4phen)	2.033 (2.015)	2.034 (2.013)	2.168 (2.120)	2.169 (2.136)
Pt(bph)(4,7-ph_2phen)	2.033 (2.015)	2.033 (2.014)	2.156 (2.133)	2.155 (2.114)
Pt(bph)(5-Clphen)	2.033	2.032	2.164	2.160

Table 3.8(b) Selected bond angles and dihedral angles (deg) from DFT optimized structures

	N-Pt-N	C-Pt-C	C-Pt-N	C-Pt-N	C-C-N-N
Pt(bph)(4-Mephen)	76.98	80.76	102.89	102.95	22.17
Pt(bph)(5-Mephen)	77.08 (76.2)	80.77 (81.3)	102.83 (107.8)	102.89 (97.9)	22.10 (19.07)
Pt(bph)(4,7-Me_2phen)	77.79 (77.4)	80.04 (79.9)	101.02 (100.1)	101.02 (102.3)	0.0 (6.48)
Pt(bph)(5,6-Me_2phen)	77.99 (76.9)	80.90 (80.1)	102.54 (103.4)	102.54 (102.5)	23.23 (20.35)
Pt(bph)(3,4,7,8- Me_4phen)	76.30 (76.8)	80.09 (80.2)	101.66 (101.3)	101.87 (102.3)	0.38 (1.86)
Pt(bph)(4,7-ph_2phen)	76.69 (77.2)	80.72 (80.5)	103.21 (104.1)	103.09 (101.1)	22.58 (21.01)
Pt(bph)(5-Clphen)	77.08	80.78	102.94	102.81	22.28

3.3.5 Electronic absorption spectra and electrochemical data

Figure 3.16 shows the electronic absorption spectra of platinum biphenyl phenanthroline complexes in butyronitrile. Figures 3.16 A and B are from different view angles. The extinction coefficients of the transitions were determined from Beer's Law studies using five dilution points and are listed in Table 3.9 as well as the wavelengths of absorption maxima and reduction potentials determined by cyclic voltammetry.

Among all eight complexes, including Pt(bph)(phen), there are three prominent bands located in the regions 400-460 nm, near 350 nm and 250-320 nm. The assignments of the experimental bands were based on computational determinations of the singlet excited states and related reports of similar types of complexes.[6] The band at 440 nm is assigned as platinum metal center to ligand charge transfer transition (MLCT). The band with strong intensity at 250-320 nm is a ligand centered π-π*transition (LC). The band around 350 nm is harder to assign and will be discussed later in the calculation part.

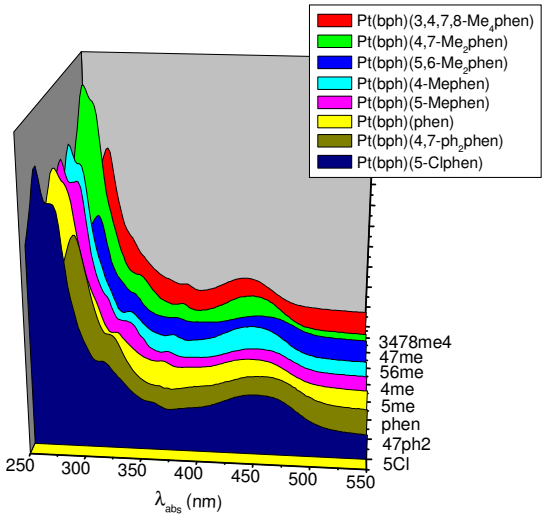

A

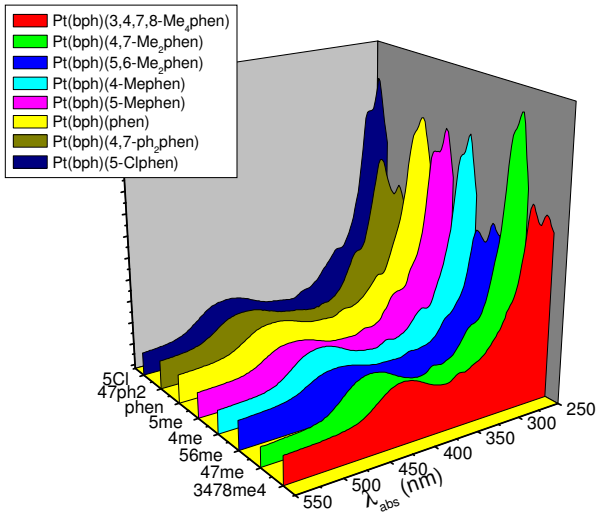

B

Figure 3.16 Electronic absorption spectra of platinum biphenyl phenanthroline derivatives in butyronitrile. A and B are from different view angles.

Table 3.9 Electronic absorption spectra and reduction potentials

	Absorbance nm ($10^3 M^{-1} cm^{-1}$)[a]				$E_{1/2red}$[b] (V)
Pt(bph)(4-Mephen)	272 (36) 258 (39)	322 (11.1)	358 (5)	438 (6.9)	-1.414
Pt(bph)(5-Mephen)	274 (39) 260 (42)	320(10.9)	356 (4.9)	442 (6.7)	-1.408
Pt(bph)(4,7-Me_2phen)	270 (51) 262 (38)	314 (11.1)	358 (4.7)	430 (7.1)	-1.408
Pt(bph)(5,6-Me_2phen)	282 (34) 260 (33)	314 (9.7)	356 (5.9)	432 (7.1)	-1.423
Pt(bph)(5-Clphen)	272 (39) 260 (37)	314 (12.4)	356 (6.1)	450 (6.8)	-1.280
Pt(bph)(3,4,7,8-Me_4phen)	278 (38) 260 (36)	310 (12.1)	358 (5.3)	422 (7.2)	not measured
Pt(bph)(4,7-ph_2phen)	284 (35) 262 (34)	314 (10.5)	356 (6.2)	448 (6.7)	-1.304

a: in butyronitrile
b: in acetonitrile

3.3.6 Correlation of Hammett sigma value with absorption and reduction potential

The Hammett sigma values of different substituents were taken from the literature.[13] Considering that the absorption, reduction potential and emission were mainly determined by the energy of the π or π* ligand orbitals, only σ_p^n, which is in the *para* position, was used to generate plots examining the relationship between these electronic properties and σ_p^n. Since the π or π* orbitals were delocalized over the whole ligand plane instead of on a specific position, the substituents in different positions were treated as in the *para* position.

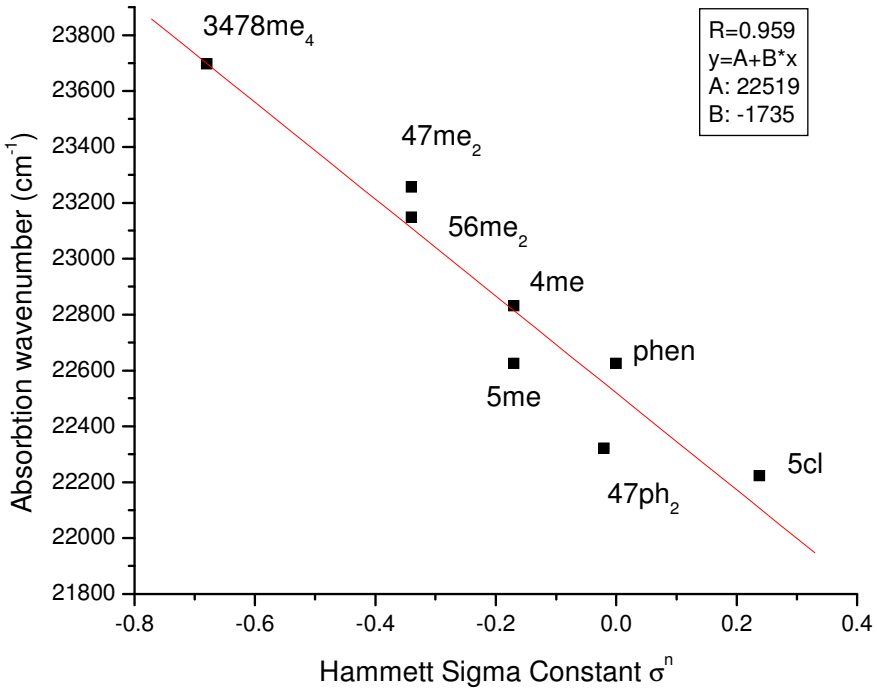

Figure 3.17 Hammett sigma value vs. λ_{max} around 440 nm

Figure 3.17 is a plot of Hammett sigma values versus absorption maxima of the MLCT bands around 440 nm. There is linear correlation between Hammett sigma values and absorption maxima. Pt(bph)(3,4,7,8-Me_4phen) having four electron donor methyl group substituents has the highest energy MLCT transition. With the electron withdrawing substituent, Cl, Pt(bph)(5-Clphen) has the lowest energy MLCT transition.

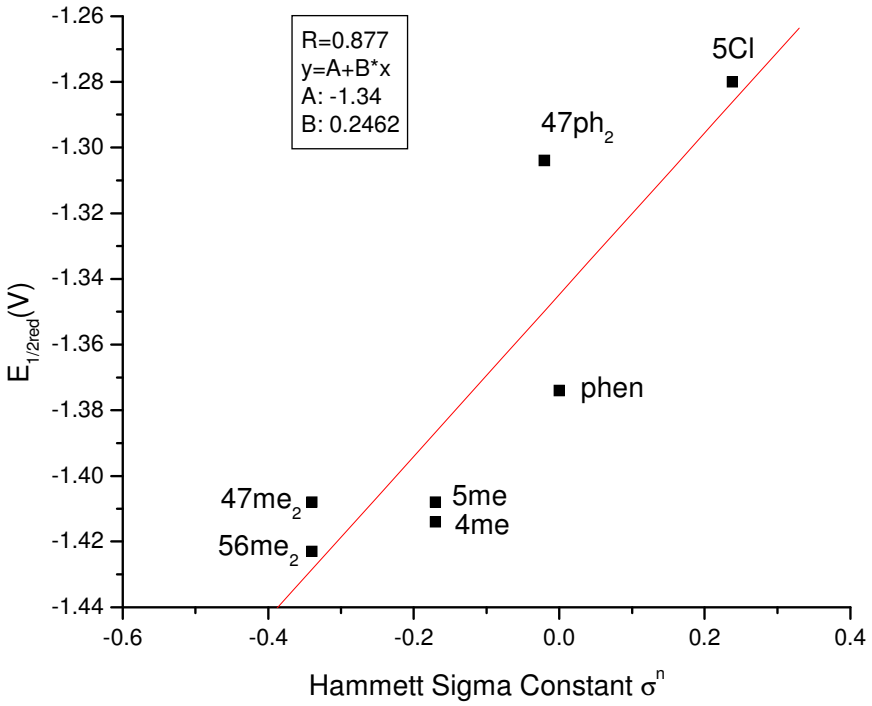

Figure 3.18 Hammett sigma value vs. $E_{1/2red}$

Figure 3.18 gives a linear correlation between Hammett sigma values and reduction potentials for the first reduction associated with adding the electron to the phen ligand. Due to the low solubility in acetonitrile, the reduction potential of Pt(bph)(3,4,7,8-Me_4phen) was not measured.

3.3.7 Population analysis

Figures 3.19-3.23 show pictures of frontier orbitals of the complexes from HOMO-3 to LUMO+3. The orbital distributions are listed in Table 3.10-3.14. All HOMOs are from the biphenyl ligand and all LUMOs are from the phenanthroline ligand. Most of L+1 to L+3 are derived from π^* orbitals located on the phenanthroline ligand except the L+3 orbital of Pt(bph)(3,4,7,8-Me_4phen) where the electron density is mainly from the *d* orbitals on the platinum metal center. Most H-1 to H-3 contain contributions from the π orbitals located on biphenyl and from *d* orbitals located on platinum, except H-3 of Pt(bph)(5,6-Me_2phen) where the π orbital contributions are from phenanthroline.

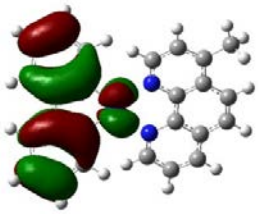

HOMO

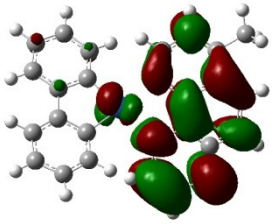

LUMO

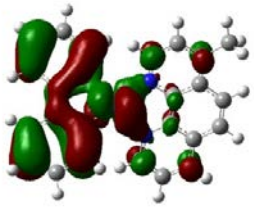

H-1

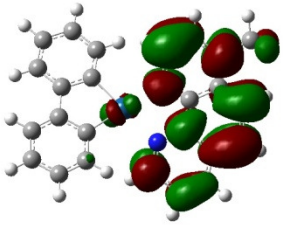

L+1

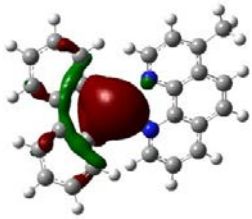

H-2

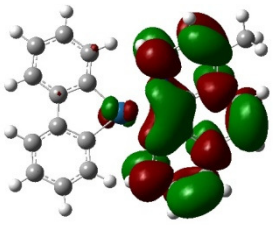

L+2

Figure 3.19 Frontier orbitals of Pt(bph)(4-Mephen)

H-3 L+3

Figure 3.19 Frontier orbitals of Pt(bph)(4-Mephen) (continued)

Table 3.10 Orbital distributions of Pt(bph)(4-Mephen)

	Energy level (eV)	Bph%	Pt%	4-Mephen%
LUMO+3	-0.55	0	2	97
LUMO+2	-1.28	2	2	96
LUMO+1	-2.55	1	1	99
LUMO	-2.61	3	5	92
HOMO	-4.62	80	19	1
HOMO-1	-5.31	50	38	11
HOMO-2	-5.47	19	80	1
HOMO-3	-5.5	79	20	1

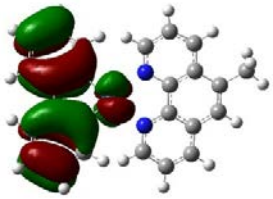

HOMO

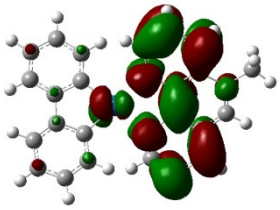

LUMO

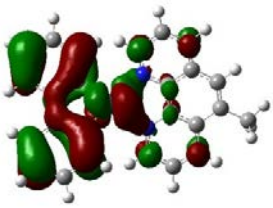

H-1

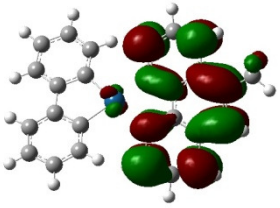

L+1

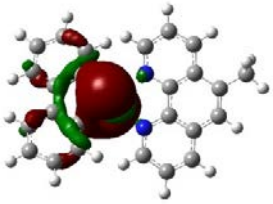

H-2

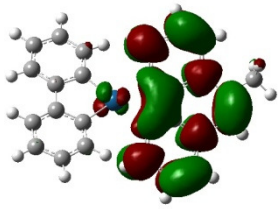

L+2

Figure 3.20 Frontier orbitals of Pt(bph)(5-Mephen) (continued)

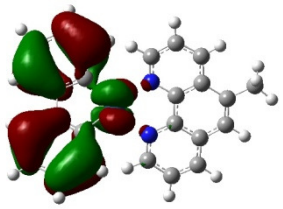

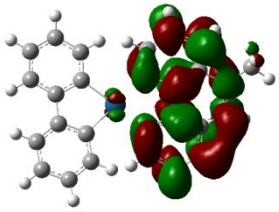

H-3 L+3

Figure 3.20 Frontier orbital of Pt(bph)(5-Mephen) (continued)

Table 3.11 Orbital distributions of Pt(bph)(5-Mephen)

	Energy level (eV)	Bph%	Pt%	5-Mephen%
LUMO+3	-0.55	0	1	99
LUMO+2	-1.29	2	2	96
LUMO+1	-2.51	1	1	99
LUMO	-2.66	3	5	92
HOMO	-4.64	80	19	1
HOMO-1	-5.35	50	38	11
HOMO-2	-5.5	19	80	1
HOMO-3	-5.52	79	20	2

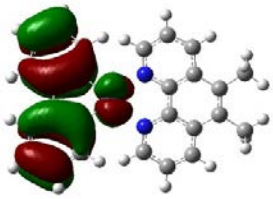

HOMO

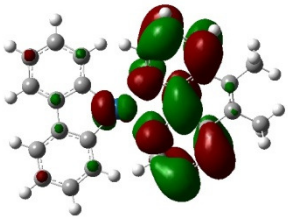

LUMO

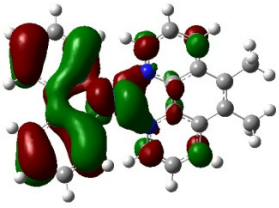

H-1

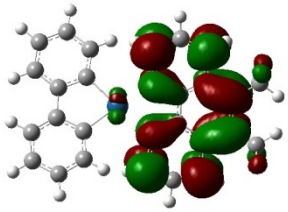

L+1

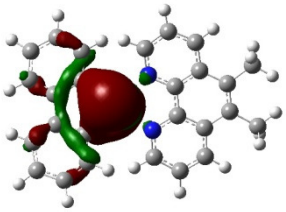

H-2

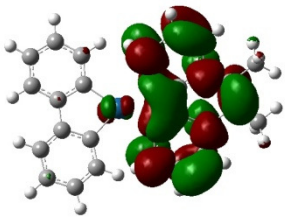

L+2

Figure 3.21 Frontier orbitals of Pt(bph)(5, 6-Me2phen)

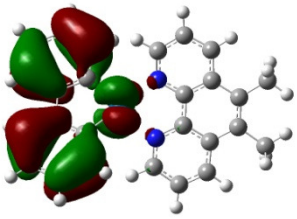

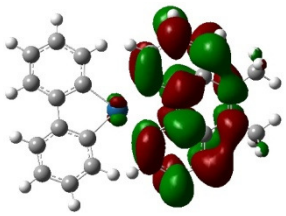

H-3 L+3

Figure 3.21 Frontier orbitals of Pt(bph)(5, 6-Me2phen) (continued)

Table 3.12 Orbital distributions of Pt(bph)(5,6-Me_2phen)

	Energy level (eV)	Bph%	Pt%	5,6-Me_2phen%
LUMO+3	-0.43	0	1	99
LUMO+2	-1.24	2	2	96
LUMO+1	-2.41	1	1	99
LUMO	-2.61	3	5	92
HOMO	-4.61	86	16	0
HOMO-1	-5.37	48	46	5
HOMO-2	-5.5	24	73	2
HOMO-3	-5.54	80	18	1

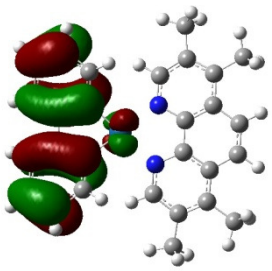

HOMO

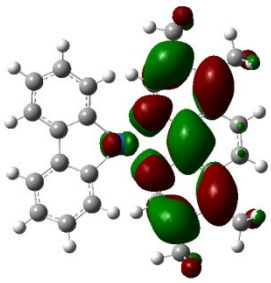

LUMO

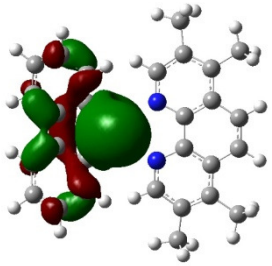

H-1

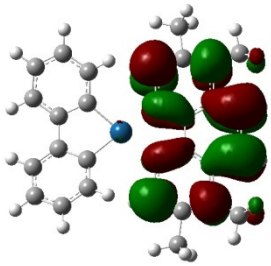

L+1

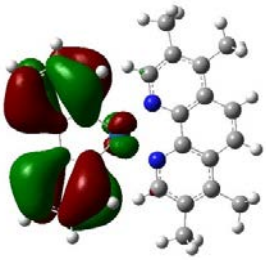

H-2

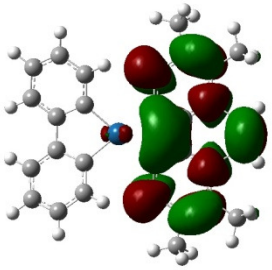

L+2

Figure 3.22 Frontier orbitals of Pt(bph)(3,4,7,8-Me4phen)

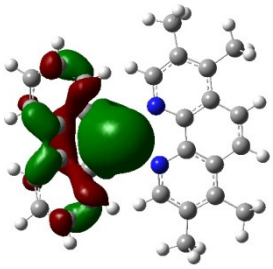

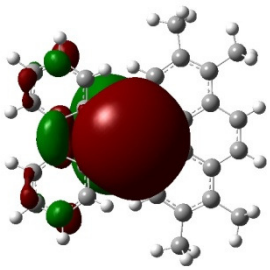

H-3 L+3

Figure 3.22 Frontier orbitals of Pt(bph)(3,4,7,8-Me4phen) (continued)

Table 3.13 Orbital distributions of Pt(bph)(3,4,7,8-Me_4phen)

	Energy level (eV)	Bph%	Pt%	3,4,7,8-Me_4phen%
LUMO+3	2.85	13	87	0
LUMO+2	2.39	2	2	96
LUMO+1	0.78	0	0	99
LUMO	0.7	1	3	96
HOMO	-6.12	96	4	0
HOMO-1	-7.42	81	15	4
HOMO-2	-7.54	94	5	1
HOMO-3	-8.51	33	67	0

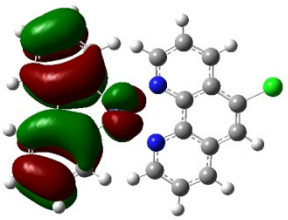

HOMO

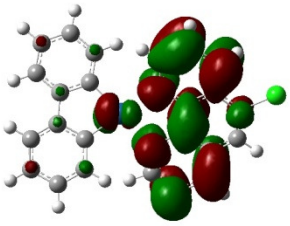

LUMO

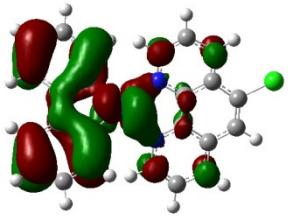

H-1

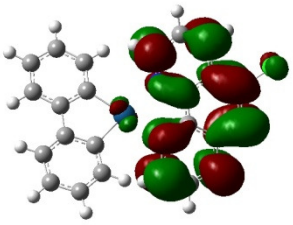

L+1

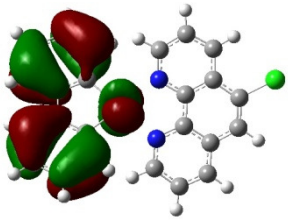

H-2

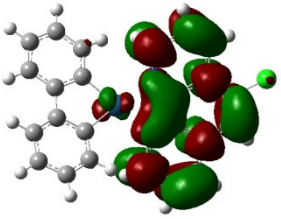

L+2

Figure 3.23 Frontier orbitals of Pt(bph)(5-Clphen)

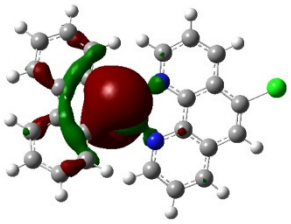

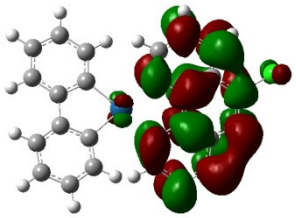

H-3 L+3

Figure 3.23 Frontier orbitals of Pt(bph)(5-Clphen) (continued)

Table 3.14 Orbital distributions of Pt(bph)(5-Clphen)

	Energy level (eV)	Bph%	Pt%	5-Clphen%
LUMO+3	-0.95	0	1	99
LUMO+2	-1.63	2	2	96
LUMO+1	-2.92	1	1	98
LUMO	-2.98	4	6	90
HOMO	-4.78	82	16	1
HOMO-1	-5.53	55	32	13
HOMO-2	-5.66	83	16	1
HOMO-3	-5.82	19	79	2

3.3.7.1 Pt(bph)(4-Mephen)

Figure 3.24 shows the overlay of experimental and calculated electronic absorption spectrum of Pt(bph)(4-Mephen). Calculated singlet energy state transitions are listed in Table 3.15. There are three predominant transitions located at 18401cm^{-1} (f = 0.1225), 39158 cm^{-1} (f = 0.124) and 39806 cm^{-1} (f = 0.465). The first transition is from the platinum metal center to 4-Mephen. The major contributions are H-1->LUMO (27%) and H-1->L+1 (37%). The transition at 39158 cm^{-1} is an intraligand π to π* transition in the 4-Mephen ligand with contributions from the H-11->LUMO (18%) and H-6->L+2 (14%). The intraligand π to π* transition from the bph ligand was located at 39806 cm^{-1} with the major contribution from H-3->L+4 (43%). The "peak" at ~27000 cm^{-1} was actully an overlay of several minority transtions like LLCT, MLCT, etc. It cannot be assigned to a specific transition. The calculated MLCT absorption was red shifted compared with the experimental spectrum. This is often found due to the gas phase TDDFTcalculations.

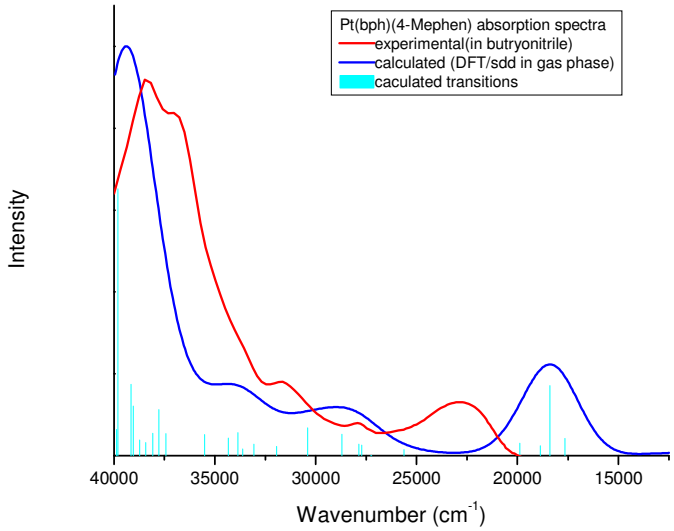

Figure 3.24 Experimental and calculated electronic absorption spectra of Pt(bph)(4-Mephen)

Table 3.15 Calculated singlet energy state transitions for Pt(bph)(4-Mephen)

ν(cm^{-1})	λ(nm)	f	Major orbital contributions	Nature of transition
18401	543	0.1225	H-1->LUMO (27%), H-1->L+1 (37%)	MLCT Pt→4-Mephen
30402	328	0.0487	HOMO->L+4 (68%)	IL $\pi\rightarrow\pi^*$ bph
33869	295	0.0403	HOMO->L+6 (57%)	LMCT bph→Pt
37771	264	0.0803	H-5->L+2 (34%)	LLCT bph→ 4-Mephen
39050	256	0.0861	H-2->L+6 (19%), H-2->L+8 (29%)	LF Pt
39158	255	0.124	H-11->LUMO (18%), H-6->L+2 (14%)	IL $\pi\rightarrow\pi^*$ 4-Mephen
39806	251	0.4655	H-3->L+4 (43%)	IL $\pi\rightarrow\pi^*$ bph
39867	250	0.0456	H-2->L+5 (58%)	MLCT Pt→4-Mephen

3.3.7.2 Pt(bph)(5,6-Me_2phen)

Figure 3.25 shows the overlay of the experimental and calculated electronic absorption spectrum of Pt(bph)(5,6-Me_2phen). Calculated singlet energy state transitions are listed in Table 3.16. There are three predominant transitions located at 17668 cm^{-1} (f = 0.1452), 38822 cm^{-1} (f = 0.1216) and 39075 cm^{-1} (f = 0.1241). The first transition is from the platinum metal center to 5,6-Me_2phen with the major contribution associated with H-1->LUMO (76%). The transition at 38822 cm^{-1} is an intraligand π to π* transition in 5,6-Me_2phen where the major contribution is H-6->L+2 (62%). The intraligand π to π* transition for the bph ligand was located at 39075 cm^{-1} with a major contributions from H-2->L+4 (25%) and H-1->L+5 (36%). The "peak" at ~29000 cm^{-1} was actully an overlay of several minority transtions like LLCT, MLCT, etc. It cannot be assigned to a specific transition. The calculated MLCT absorption was red shifted compared with the experimental spectrum. This is often found due to the gas phase TDDFTcalculations.

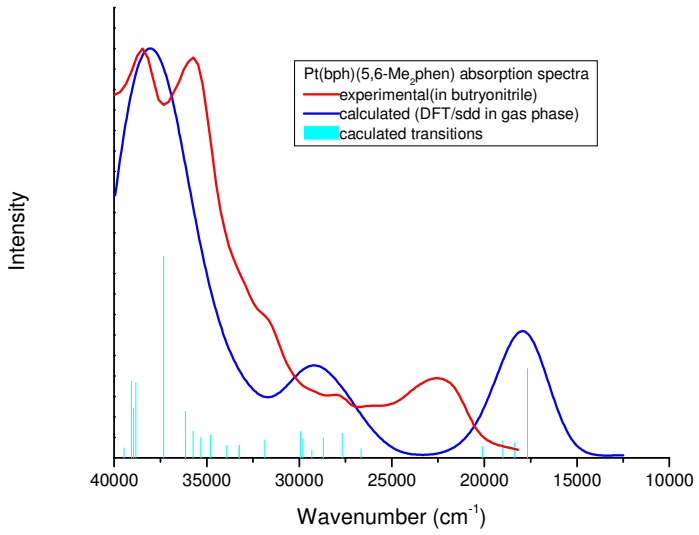

Figure 3.25 Experimental and calculated electronic absorption spectra of Pt(bph)(5,6-Me_2phen)

Table 3.16 Calculated singlet energy state transitions for Pt(bph)(5,6-M_2ephen)

ν(cm^{-1})	λ(nm)	f	Major orbital contributions	Nature of transition
17668	566	0.1452	H-1->LUMO (76%)	MLCT Pt,bph→5,6-Me_2phen
29933	334	0.0425	HOMO->L+4 (46%)	LLCT bph→5,6-Me_2phen
35723	280	0.0435	H-11->L+1 (49%)	LLCT bph→5,6-Me_2phen
36159	277	0.0754	H-2->L+3 (63%)	MLCT Pt→ 5,6-Me_2phen
37336	268	0.3283	H-11->LUMO (39%)	MLCT Pt,bph→5,6-Me_2phen
38822	258	0.1216	H-6->L+2 (62%)	IL $\pi\rightarrow\pi^*$ 5,6-Me_2phen
38947	257	0.0814	H-1->L+5 (61%)	LMCT bph→ Pt
39075	256	0.1241	H-1->L+5 (36%)	LMCT bph→Pt
40120	249	0.0574	H-3->L+6 (72%)	LF Pt
40124	249	0.0525	H-3->L+5 (40%)	IL $\pi\rightarrow\pi^*$ bph

3.3.7.3 Pt(bph)(4,7-Me_2phen)

Figure 3.26 shows the overlay of experimental and calculated electronic absorption spectrum of Pt(bph)(4,7-Me_2phen). The calculated singlet energy state transitions are listed in Table 3.17. There are five predominant transitions located at 18965 cm^{-1} (f = 0.1314), 28574 cm^{-1} (f = 0.1243), 37084 cm^{-1} (f = 0.1274), 38555 cm^{-1} (f = 0.2149) and 39172 cm^{-1} (f = 0.4225). The transition at 18965 cm^{-1} is from the platinum metal center to 4,7-Me_2phen where the major contribution is associated with H-1->LUMO (49%). The transition at 28574 cm^{-1} is an interligand π to π* transition from bph to 4,7-Me_2phen where the major contributions are H-1->L+2 (22%) and HOMO->L+3 (30%). The intraligand π to π* transition for the 4,7-Me_2phen ligand were locate at 37084 cm^{-1} and 38555 cm^{-1} with major contributions from H-11->L+1 (47%) and H-11->LUMO (35%). The intraligand π to π* transition of bph was located at 39172 cm^{-1}. The calculated MLCT absorption was red shifted compared with the experimental spectrum. This is often found due to the gas phase TDDFTcalculations.

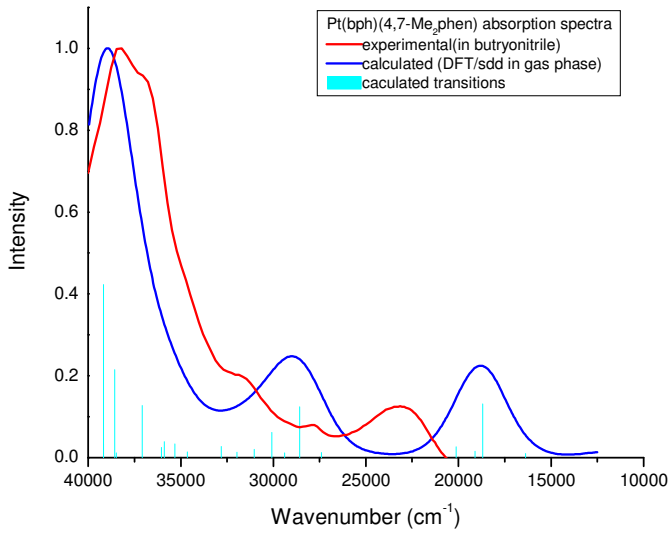

Figure 3.26 Experimental and calculated electronic absorption spectra of Pt(bph)(4,7-Me_2phen)

Table 3.17 Calculated singlet energy state transitions for Pt(bph)(4,7-Me_2phen)

ν(cm^{-1})	λ(nm)	f	Major orbital contributions	Nature of transition
18695	535	0.1314	H-1->LUMO (49%)	MLCT Pt→4,7-Me_2phen
28574	350	0.1243	H-1->L+2 (22%), HOMO->L+3 (30%)	LLCT bph→4,7-Me_2phen
30079	332	0.0615	HOMO->L+4 (55%)	MLCT Pt,bph→4,7-Me_2phen
37084	270	0.1274	H-11->L+1 (47%)	IL $\pi\rightarrow\pi^*$ 4,7-Me_2phen
38555	259	0.2149	H-11->LUMO (35%)	IL $\pi\rightarrow\pi^*$ 4,7-Me_2phen
39172	255	0.4225	H-2->L+4 (55%)	IL $\pi\rightarrow\pi^*$ bph
40356	248	0.0471	H-3->L+6 (41%), HOMO->L+8 (-22%)	LMCT bph→ Pt
40951	244	0.0685	H-1->L+7 (60%)	LLCT bph→ 4,7-Me_2phen

3.3.7.4 Pt(bph)(3,4,7,8-Me_4phen)

Figure 3.27 shows the overlay of experimental and calculated electronic absorption spectrum of Pt(bph)(3,4,7,8-Me_4phen). The calculated singlet energy state transitions are listed in Table 3.18. There are five predominant transitions locat at 19566 cm^{-1} (f = 0.1186), 29513 cm^{-1} (f = 0.1015), 36150 cm^{-1} (f = 0.2273), 38165 cm^{-1} (f = 0.2445) and 39105 cm^{-1} (f = 0.3771). The transition at 19566 cm^{-1} is from the platinum metal center to 3,4,7,8-Me_4phen where the major contribution is H-1->L+1 (44%). The transition at 29513 cm^{-1} was a combination of MLCT from Pt to 3,4,7,8-Me_4phen and a LLCT from bph to 3,4,7,8-Me_4phen. The major contributions are H-6->L+1 (24%) and H-2->L+2 (23%). The intraligand π to π* transition of 3,4,7,8-Me_4phen was located at 36150 cm^{-1} with major contributions from H-10->L+1 (23%) and H-5->L+2 (34%). The intraligand π to π* transition from bph ligand was locate at 39105 cm^{-1} with the major contribution of H-3->L+4 (65%). The transition at 38165 cm^{-1} was also a combination

of MLCT from Pt to 3,4,7,8-Me_4phen and a LLCT from bph to 3,4,7,8-Me_4phen with the major contribution H-5->L+2 (60%). The calculated MLCT absorption was red shifted compared with the experimental spectrum. This is often found due to the gas phase TDDFTcalculations.

Table 3.18 Calculated singlet energy state transitions for Pt(bph)(3,4,7,8-Me_4phen)

ν(cm^{-1})	λ(nm)	f	Major orbital contributions	Nature of transition
19566	511	0.1186	H-1->L+1 (44%)	MLCT Pt→3,4,7,8-Me_4phen
20626	485	0.0586	H-3->LUMO (77%)	LLCT bph→3,4,7,8-Me_4phen
29513	339	0.1015	H-6->L+1 (24%), H-2->L+2 (23%)	MLCT Pt,bph→3,4,7,8-Me_4phen
29730	336	0.0617	HOMO->L+4 (74%)	IL $\pi\rightarrow\pi^*$ bph
33492	299	0.0683	H-11->L+1 (42%)	IL $\pi\rightarrow\pi^*$ 3,4,7,8-Me_4phen
35831	279	0.0868	H-2->L+4 (49%)	MLCT Pt→ bph
35858	279	0.0445	H-11->L+1 (23%), H-2->L+4 (27%)	MLCT Pt,bph→3,4,7,8-Me_4phen
36150	277	0.2273	H-10->L+1 (23%), H-5->L+2 (34%)	IL $\pi\rightarrow\pi^*$ 3,4,7,8-Me_4phen
38165	262	0.2445	H-5->L+2 (60%)	MLCT Pt,bph→3,4,7,8-Me_4phen
39105	256	0.3771	H-3->L+4 (65%)	IL $\pi\rightarrow\pi^*$ bph

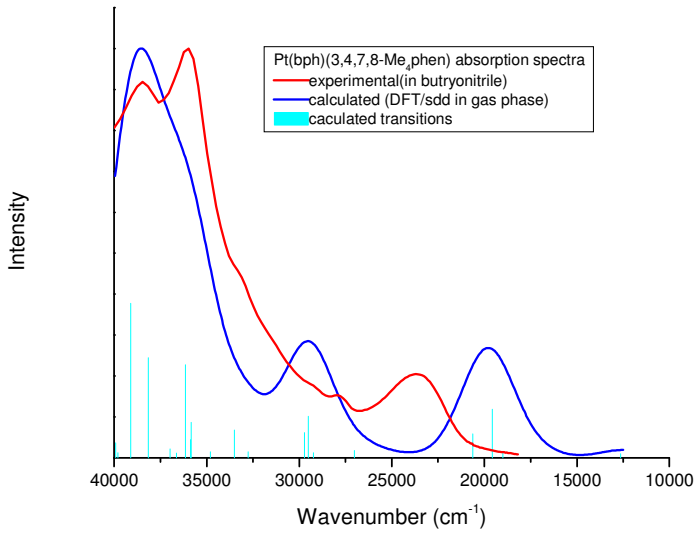

Figure 3.27 Experimental and calculated electronic absorption spectra of Pt(bph)(3,4,7,8-Me4phen)

3.3.7.5 Pt(bph)(5-Clphen)

Figure 3.28 shows the overlay of experimental and calculated electronic absorption spectrum of Pt(bph)(5-Clphen). The calculated singlet energy state transitions are listed in Table 3.19. There are three predominant transitions located at 17081 cm^{-1} (f = 0.1132), 37730 cm^{-1} (f = 0.1976) and 39119 cm^{-1} (f = 0.3401). The first transition is from the platinum metal center to 5-Clphen. Here the major contribution is H-1->LUMO (62%). The transition at 37730 cm^{-1} was a mixture of MLCT and LLCT from Pt and bph to 5-Clphen where the contributions are H-11->LUMO (25%) and H-3->L+4 (24%). The intraligand π to π* transition from bph ligand was located at 39119 cm^{-1} with its major contribution from H-2->L+5 (55%). The "peak" at ~27000 cm^{-1} was actully an mixture of several minority transtions like LLCT, MLCT, etc. It cannot be assigned to a specific transition. The calculated MLCT absorption was red shifted compared with the experimental spectrum. This is often found due to the gas phase TDDFTcalculations.

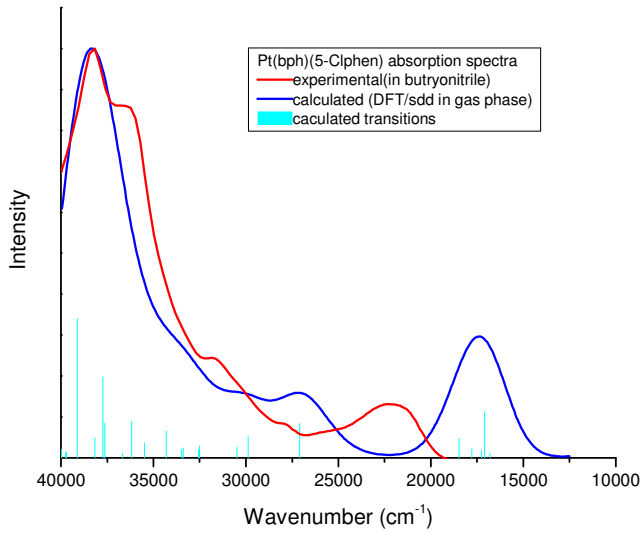

Figure 3.28 Experimental and calculated electronic absorption spectra of Pt(bph)(5-Clphen)

Table 3.19 Calculated singlet energy state transitions for Pt(bph)(5-Clphen)

ν(cm^{-1})	λ(nm)	f	Major orbital contributions	Nature of transition
17081	585	0.1132	H-1->LUMO (62%)	MLCT Pt→5-Clphen
18481	541	0.0474	H-2->L+1 (66%)	MLCT Pt,bph→5-Clphen
27096	369	0.0835	H-1->L+2 (53%), HOMO->L+3 (-34%)	MLCT Pt,bph→5-Clphen
29870	335	0.0527	HOMO->L+5 (72%)	IL $\pi\rightarrow\pi^*$ bph
34305	291	0.0644	H-2->L+3 (51%)	LLCT bph→5-Clphen
36176	276	0.0895	H-11->L+1 (42%)	IL $\pi\rightarrow\pi^*$ 5-Clphen
37628	266	0.0845	H-3->L+4 (55%)	MLCT Pt→5-Clphen
37730	265	0.1976	H-11->LUMO (25%), H-3->L+4 (24%)	MLCT Pt,bph→5-Clphen
38170	262	0.0497	H-6->L+2 (79%)	MLCT Pt,bph→5-Clphen
39119	256	0.3401	H-2->L+5 (55%)	IL $\pi\rightarrow\pi^*$ bph

3.3.8 Emission spectra

Emission spectra at 77K are shown in Figure 3.29 in two different view angles. The emission maxima, quantum yields and emission lifetimes are listed in Table 3.20. The emission of eight platinum biphenyl phenanthroline derivative complexes can be divided into three groups: Group I: Pt(bph)(5,6-Me_2phen) with highly resolved vibronic structure, Group II: Pt(bph)(phen) and Pt(bph)(5-Clphen) without vibronic structure but with narrow band width, and Group III: Pt(bph)(4-Mephen), Pt(bph)(5-Mephen), Pt(bph)(4,7-Me_2phen), Pt(bph)(4,7-ph_2phen) and Pt(bph)(3,4,7,8-Me_4phen) with no vibronic structure and broad band width.

Figure 3.30 shows the correlation between Hammett sigma values and emission maxima. Group I: Pt(bph)(5,6-Me_2phen) has the highest emission maximum energy of 20600cm^{-1}. Group II: Pt(bph)(phen) and Pt(bph)(5-Clphen) have medium emission energies of ~17000cm^{-1} and Group III: Pt(bph)(4-Mephen), Pt(bph)(5-Mephen), Pt(bph)(4,7-Me_2phen), Pt(bph)(4,7-ph_2phen) and Pt(bph)(3,4,7,8-Me_4phen) have the lowest emission energies of ~16000cm^{-1}. In Group III there is a good linear relationship between Hammett sigma values and emission energy maxima.

The emissions of different groups have different origins. In Figure 3.31, for group I, the highly resolved vibronic structure usually comes from ligand centered transitions. Group II has narrow band width and the emission maximum of Pt(bph)(phen) does not change much with various solvents. This indicates group II is associated with a ligand field transition. Group III has a broad, unstructured emission profile which is consistent with metal to ligand charge transfer caused by coupling of the metal-ligand vibronic modes making the emission band broader.

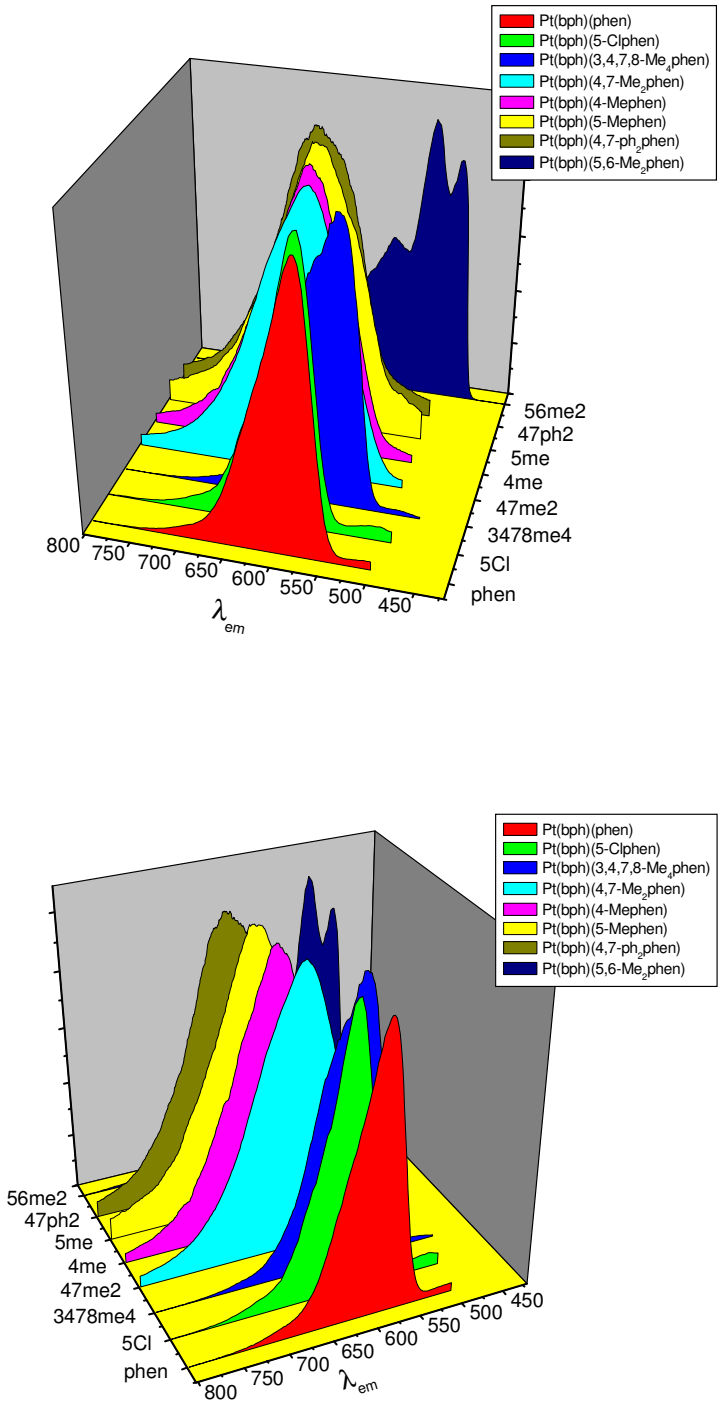

Figure 3.29 Emission spectra of platinum biphenyl phenanthroline derivatives at 77K in butyronitrile

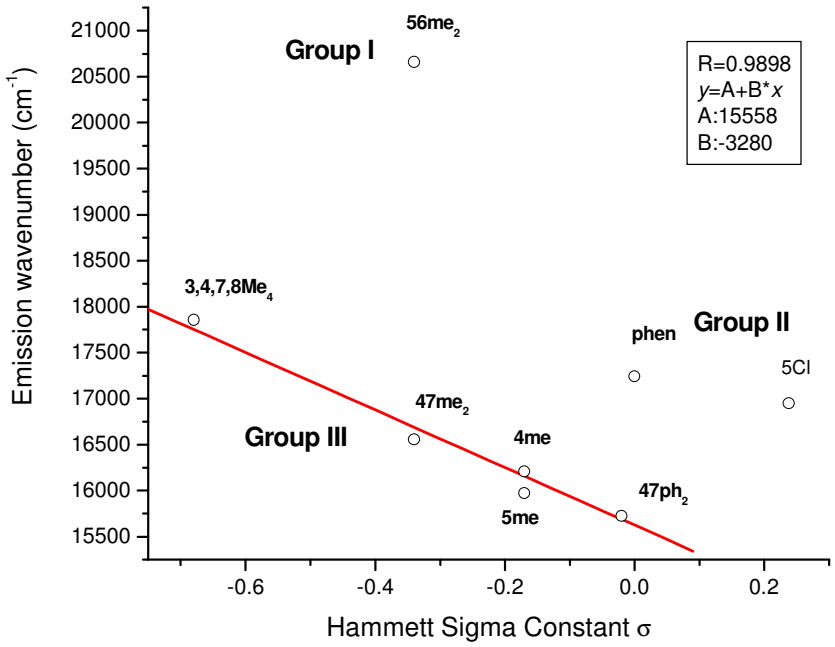

Figure 3.30 Linear relationship of Hammett sigma values with emission maxima in group III

Table 3.20 Emission properties at 77K and room temperature

	λ_{em}(nm) 77K	Φ_{em}^{a} (10^{-3}) R.T.	τ^{b} (μs) R.T.
Pt(bph)(phen)	580	1.83	3.34
Pt(bph)(4-Mephen)	617	0.089	2.97
Pt(bph)(5-Mephen)	626	0.128	2.29
Pt(bph)(4,7-Me_2phen)	604	0.13	3.93
Pt(bph)(5,6-Me_2phen)	484	0.096	1.82
Pt(bph)(3,4,7,8-Me_4phen)	560	2.95	4.89
Pt(bph)(4,7-ph_2phen)	636	0.12	1.86
Pt(bph)(5-Clphen)	590	0.70	1.83

a:excited at 450nm
b:excited at 355nm

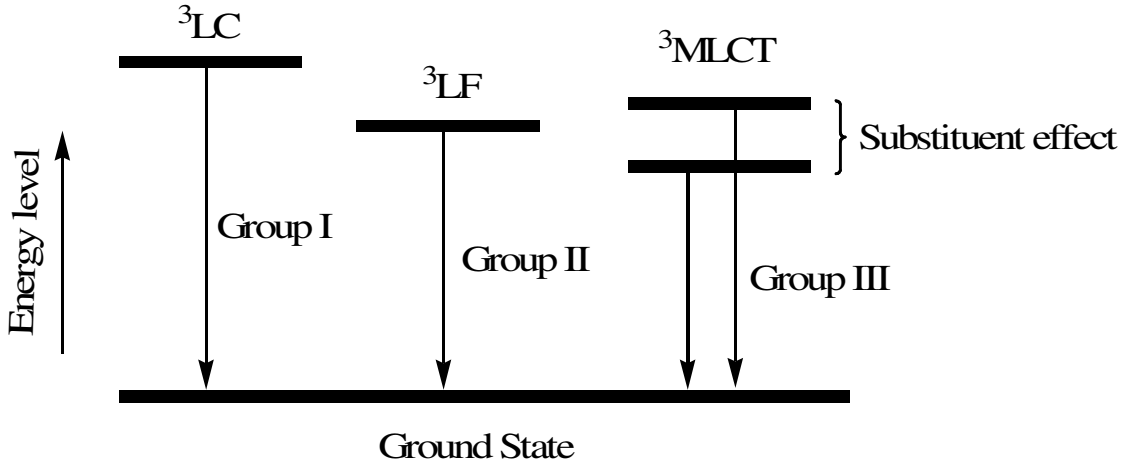

Figure 3.31 Energy level diagram of excited states associated with the substituent effect

The emission life times of the complexes were in the scale of microseconds. Pt(bph)(3,4,7,8-Me_4phen) had the longest life time, 4.89 μs and Pt(bph)(5,6-Me_2phen) had the shortest at 1.82 μs. Again the life times of members from group III have linear correlation with Hammett sigma value as shown in Figure 3.32. R = 0.959 and slope is -4.674.

A linear relationship was not found between quantum yield and Hammett sigma values. Pt(bph)(3,4,7,8-Me_4phen) also had the highest quantum yield 2.95 x 10^{-3}. Pt(bph)(4-Mephen) had the lowest quantum yield 8.9 x 10^{-5}.

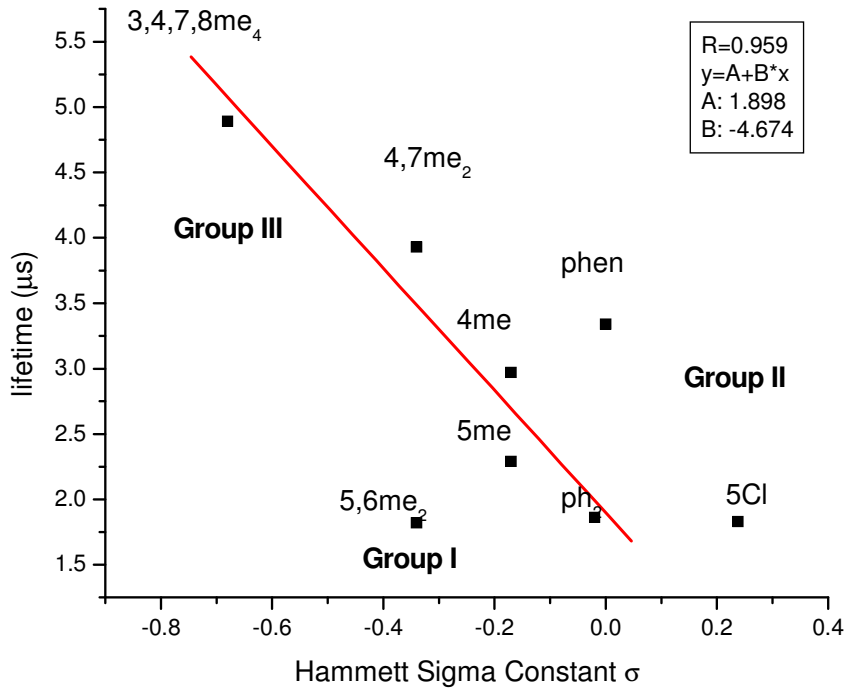

Figure 3.32 Linear relationship of Hammett sigma values with emission life time in group III

3.4 Conclusion

Seven platinum biphenyl phenanthroline derivatives were synthesized and characterized. ^{1}H NMR signals of protons on ligand rings were assigned. Five crystal structures were obtained. Three of them were in the X configuration and two were in the B configuration. The optimized structure was carried out by DFT. The MLCT bands in absorption spectra were from platinum to phenanthroline ligand instead of bph. The MLCT also had a linear relationship with Hammett sigma values. The origin of emission at 77 K can be divided into three groups: LC, LF and MLCT. Each group had a different emission profile shape and different correlations with Hammett sigma values.

REFERENCES

REFERENCES

1. Balzani, V,; Moggi, L. *Coord. Chem. Rev.* **1990**, 97, 313.

2. Meyer, T. J. *Acc. Chem. Res.* **1989**, 22, 163-170.

3. Balzani, V,; Scandola, F. *Supermolecular Photochemistry*; Ellis Horword: Chichester, UK, **1991**.

4. Cheng, L.; Tam, W.; Eaton, D. F. *Organometallics* **1990**, 9, 2856-2857.

5. Prasad, P. N.; Reinhardt, B. A. *Chem. Mater*. **1990**, 2, 660-669.

6. Friendman, A. E.; Chambron, J.; Sauvage, J.; Turro, N. J.; Barton, J. K. *J. Am. Chem. Soc.* **1990**, 112, 4960.

7. Juris, A.; Balzani, V.; Barigelletti, F.; Campagna, S.; Belser, P.; Von Zelewsky, A. *Coord. Chem. Rev.* **1988**, 84, 85.

8. Stacy, N. E.; Conner, K. A,; McMillin, D. R.; Walton, R. A. *Inorg. Chem*. **1986**, 25, 3649.

9. Patterson, H. H.; Tewksbury, J. C.; Martin, M.; Krogh-Jesperson, B.; LoMenzo, J. A.; Hooper, H. O.; Viswanath, A. K. *Inorg.Chem*. **1981**, 20, 2297.

10. Miskowski, V. M; Houlding, V. H. *Inorg. Chem*. **1989**, 28, 1529-1533.

11. Definition IUPAC gold book **1996**.

12. Keenan, S. L.; Peterson, K. P.; Peterson, K.; Jacobson, K. *J. Chem. Educ*. **2008**, 85, 558.

13. Gordon, A. J.; Ford, R. A. *The Chemist's Companion*; **1972**, John Wiley & Sons.

14. Chen, Y.; Merkert, J. W.; Murtaza, Z.; Woods, C.; Rillema, D. P. *Inorg. Chim. Acta* **1995**, 240, 41.

15. Blanton, C. B.; Murtaza, Z.; Shaver, R. J.; Rillema, D. P. *Inorg.Chem*. **1992**, 31, 3230.

16. Rillema, D. P.; Taghdiri, D. G.; Jones, D. S.; Keller, C. D.; Worl, L. A.; Meyer, T. J.; Levy, H. A. *Inorg Chem*. **1987**, 26, 578.

17. Rillema, D. P.; Mack, K. B. *Inorg. Chem*. **1982**, 21, 3849.

18. Rillema, D. P.; Callahan, R. W.; Mack, K. B. *Inorg. Chem*. **1982,** 21, 2589.

19. Cornioley-Deuschel, C; von Zelewsky, A. *Inorg.Chem*. **1987**, 26, 3354.

20. Blanton, C. B.; Rillema, D. P. *Inorg. Chim. Acta* **1990**, 168, 145.

21. Houlding, V. H.; Miskowsky, V. M. *Coord. Chem. Rev*. **1991**, 111, 145

22. (a)Becker, A. D. *J. Chem. Phys.* **1993**, 98, 5648. (b) Lee, C.; Yang, W.; Parr, R. G. *Phys. Rev. B* **1988**, 37, 785. (c) Vosko, S. H.; Wilk, L.; Nusair, M. Can. *J. Phys.* **1980**, 58, 1200. (d) Andrae, D.; Hauessermann, U.; Dolg, M.; Stoll, H.; Preuss, H. *Theor. Chim. Acta* **1990**, 77, 123.

23. (a)Stratmann, R. E.; Scuseria, G. E.; Frisch, M. *J. Chem. Phys.* **1998**, 109, 8218. (b)Bauernschmitt, R.; Ahlrichs, R. *Chem. Phys. Lett.* **1996**, 256, 454. (c) Casida, M. E.; Jamorski, C.; Casida, K. C.; Salahub, D. R. *J. Chem. Phys.* **1998**, 108, 4439.

24. (a)Cossi, M.; Barone, V. *J. Chem. Phys.* **2001**, 115, 4708. (b) Barone, V.; Cossi, M. *J. Phys. Chem. A* **1998**, 102, 1995. (c)Cossi, M.; Rega, N.; Scalmani, G.; Barone, V. *J. Comput. Chem.* **2003**, 24, 669.

25. Gilman, H.; Gaj, B. J. *J. Org. Chem*. **1957**, 22, 447.

26. Gardner, S. A.; Gordon, H. B.; Rausch, M. D. *J. Organomet. Chem*. **1973**, 60, 179.

27. Kauffmann, G. B.; Cowan, D. O. *Inorg. Synth*. **1960**, 6, 211.

28. (a)Bruker *APEX2 User Manul* 2006, Brucker AXS Inc., Madison, Wisconsin, USA. (b)Schdrick, G. M. *SHELXS97 and SHELXL97* **1997**, University of Gottingen, Germany.

29. Mdleleni, M. M.; Bridgewater, J. S.; Watts, R. J.; Ford, P. C. *Inorg. Chem*. **1995**, 34, 2334.

30. Chassot, L.; Muller, E.; von Zelewsky, A. *Inorg. Chem*. **1984**, 23, 4249.

31. Dong, V.; Keller, H. J.; Moroni, W.; Nothe, D. *Acta Crystallgr., Sect. B: Struct. Crystallogr. Cryst. Chem.* **1977**, B33, 2428.

32. Endres, H.; Keller, H. J.; Moroni, W.; Nothe, D.; Dong, V. *Acta Crystallgr., Sect. B: Struct. Crystallogr. Cryst. Chem.* **1978**, B34, 1823.

33. Hazell, A.; Mukhopadhyay, A. *Acta Crystallogr., Sect. B: Struct. Crystallogr. Cryst. Chem*. **1980**, B36, 1647.

34. Maestri, M.; Sandrini, D.; Balzani, V.; von Zelewsky, A.; Cornioley-Deuschel, C; Jolliet, P. *Helv.Chim. Acta* **1988**, 71, 1053.

35. (a) Caspar, J. V. Ph.D. Thesis, University of North Carolina, Chapel Hill, North Carolina, **1982**. (b) Allen, G. H.; White, R. P.; Rillema, D. P.; T. J. *J. Am. Chem. Soc*. **1984**, 106, 2613.

36. Hazell, A.; Simonsen, O.; Wernberg, O. *Acta Crystallogr., Sect. C* **1986**, 42, 1707.

37. Rund, J. V.; Hazell, A. C. *Acta Crystallogr., Sect. B: Struct. Crystallogr. Cryst. Chem.* **1980**, B36, 3103.

38. Herber, R. H.; Croft, M.; Coyer, M. J.; Bilash, B.; Sahiner, A. *Inorg. Chem*. **1994**, 33, 2422.

39. Mdleleni, M. M.; Bridgewater, J. S.; Watts, R. J.; Ford, P. C. *Inorg. Chem.* **1995**, *34*, 2334.

40. Chassot, L.; Muller, E.; von Zelewsky, A. *Inorg. Chem.* **1984**, *23*, 4249.

41. Ballardini, R.; Varani, G.; Indelli, M. T.; Scandola, F. *Inorg. Chem.* **1986,** 25, 3858.

42. Sykora, J.; Sima, J. *Coord. Chem. Rev.* **1990**, 107, 1.